Spin transitions in Fe

Fairy-tale I: What are the spin transitions?

Fairy-tale II: Changes of physical properties in the lower-mantle minerals?

Geodynamic story:

- Radiative transfer of heat at the bottom of the mantle?
- Other “asthenospheres” in the lower mantle?
- A viscosity hill in the lower mantle?

Hyperfine Interact
DOI 10.1007/s10751-011-0420-7

Electronic spin transition of iron in the Earth's lower mantle

Jung-Fu Lin · Andrea Wheat

Abstract Silicate perovskite and ferropericlase are thought to be the primary constituents of the lower mantle, whereas silicate post-perovskite is more likely found in the lowermost mantle. Because these minerals contain certain amounts of iron, their properties and, consequently, those of the deep mantle, are strongly influenced by iron's spin and valence states. A high-spin to low-spin crossover in ferropericlase has been observed to occur in the middle part of the lower-mantle conditions. Recent Mössbauer results consistently show that Fe^{2+} predominantly exhibits extremely high quadrupole splittings in perovskite and post-perovskite, whereas a high-spin to low-spin transition of Fe^{3+} in the octahedral site occurs at high pressures. These results provide a new venue for discussion of the effects of the spin and valence states of iron on the physical and chemical properties of the lower mantle.

Published online: 01 November 2011

Springer

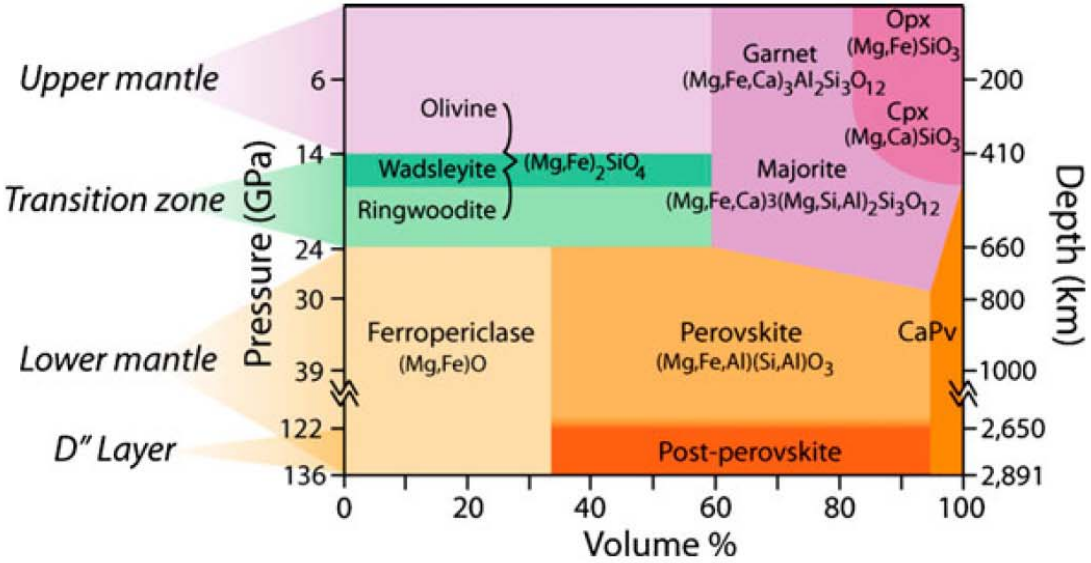

Fig. 1 Approximate mineral distribution within Earth's interior as a function of depth, pressure and volume%. Mineral abbreviation: Opx and cpx, orthopyroxene and clinopyroxene, respectively; CaPv, calcium silicate perovskite

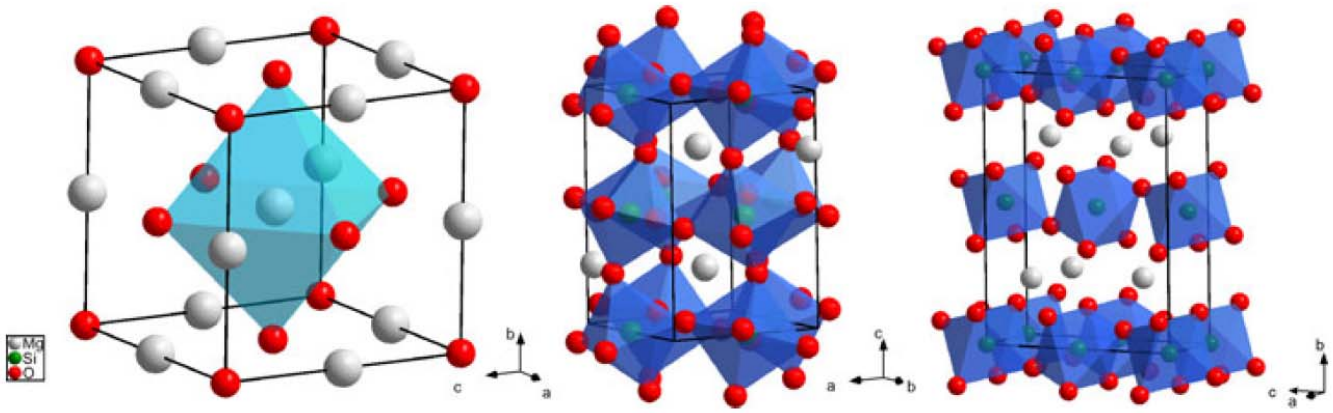

Fig. 2 Crystal structures of lower-mantle ferropericlase (*left*), silicate perovskite (*middle*), and silicate post-perovskite (*right*). Cubic ferropericlase is in the rock salt structure ($Fm\bar{3}m$); orthorhombic perovskite is in the *Pbnm* space group; orthorhombic post-perovskite is in the *Cmcm* space group

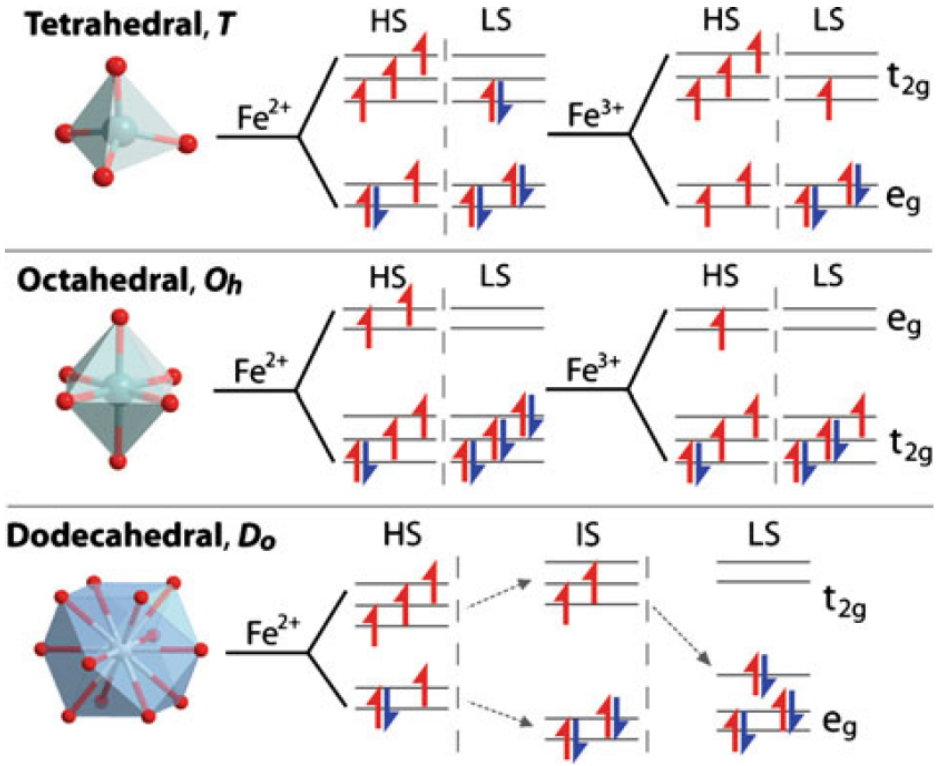

Fig. 3 Crystal field splitting diagrams for iron in tetrahedral, octahedral, and dodecahedral sites in the lower-mantle minerals. Iron is shown as a (2+) or (3+) cation in high-spin, intermediate-spin (dodecahedral site), and low-spin electronic configurations. The crystal field splitting energy (CFSE) can be altered by pressure, temperature, and/or composition. The energy of the e_g orbitals (those which are oriented towards the ligands) is heightened by increased repulsion due to shortened e_g orbital-ligand distance during pressure-induced unit cell distortion, resulting in an overall larger CFSE. When the CFSE surpasses the spin-pairing energy, the spin-pairing transition of 3*d* electrons is more favorable than jumping the energy gap to achieve aligned spins. For example, the low-spin state with all six 3*d* electrons paired ($S = 0$) in Fe^{2+} occurs at high pressures in the lower-mantle ferropericlase

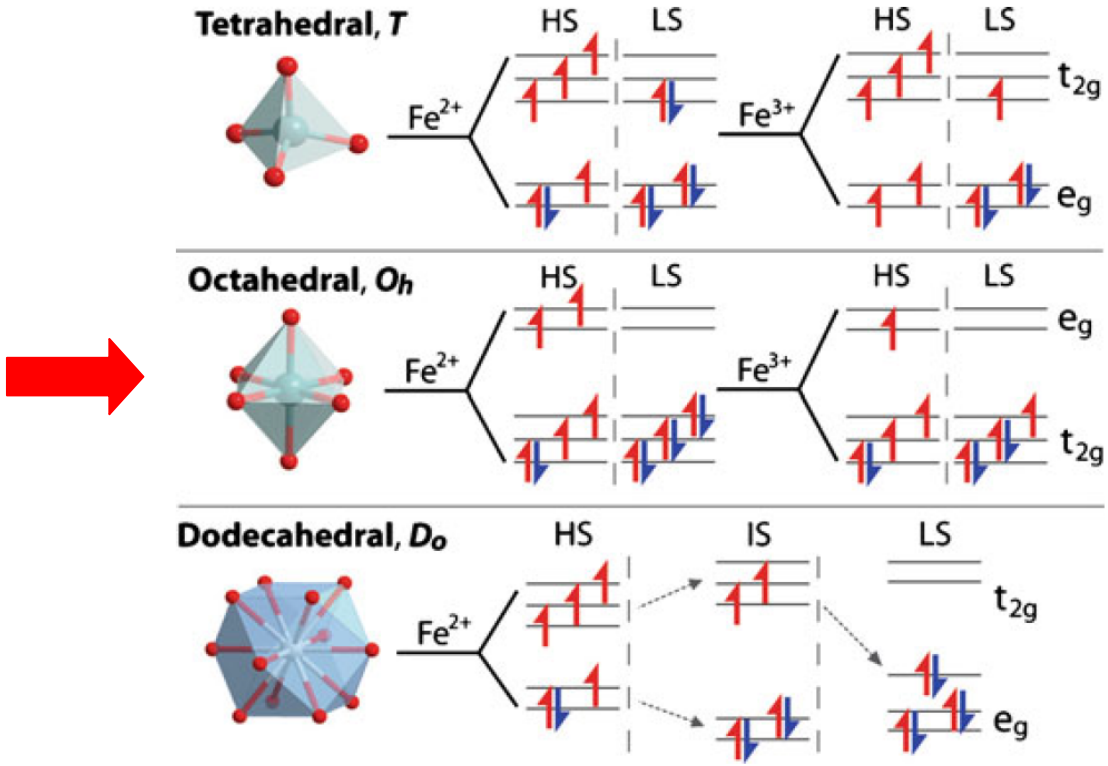

(Mg,Fe)O: HS → LS at 60 GPa

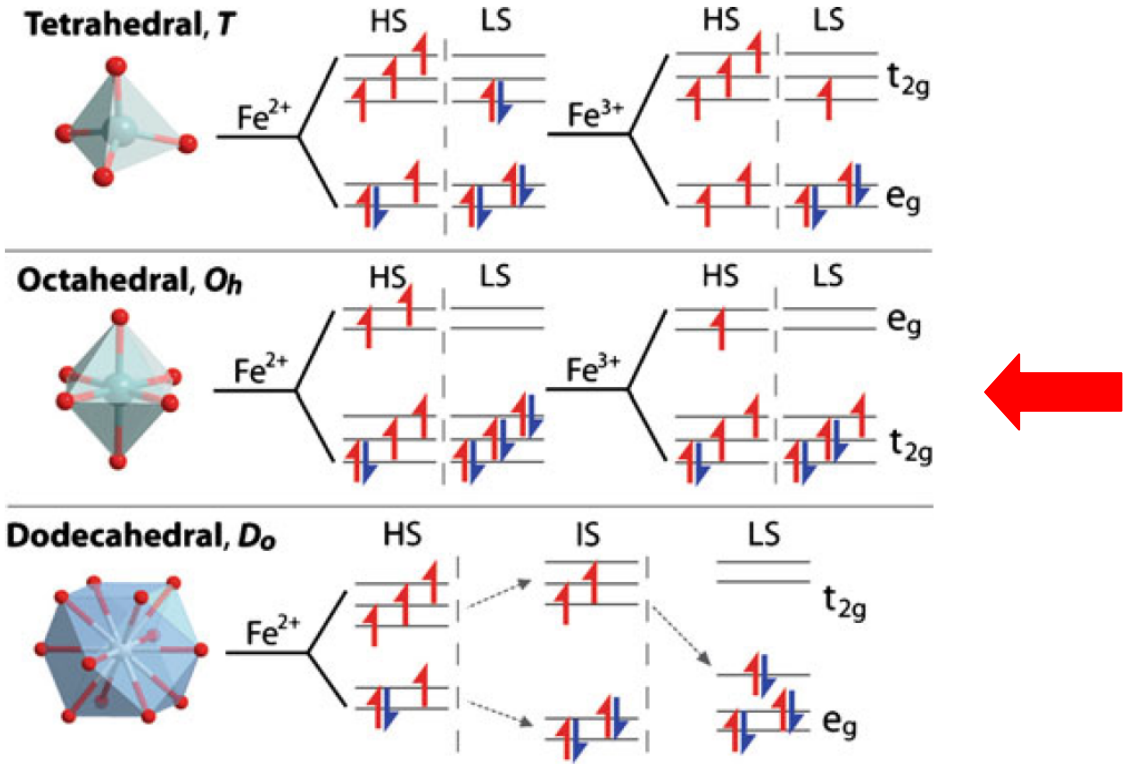

(Mg,Fe)SiO3:

HS → LS at 50-60 GPa if Fe occupies the Si site
no HS → LS up to 136 GPa if Fe occupies the Mg site

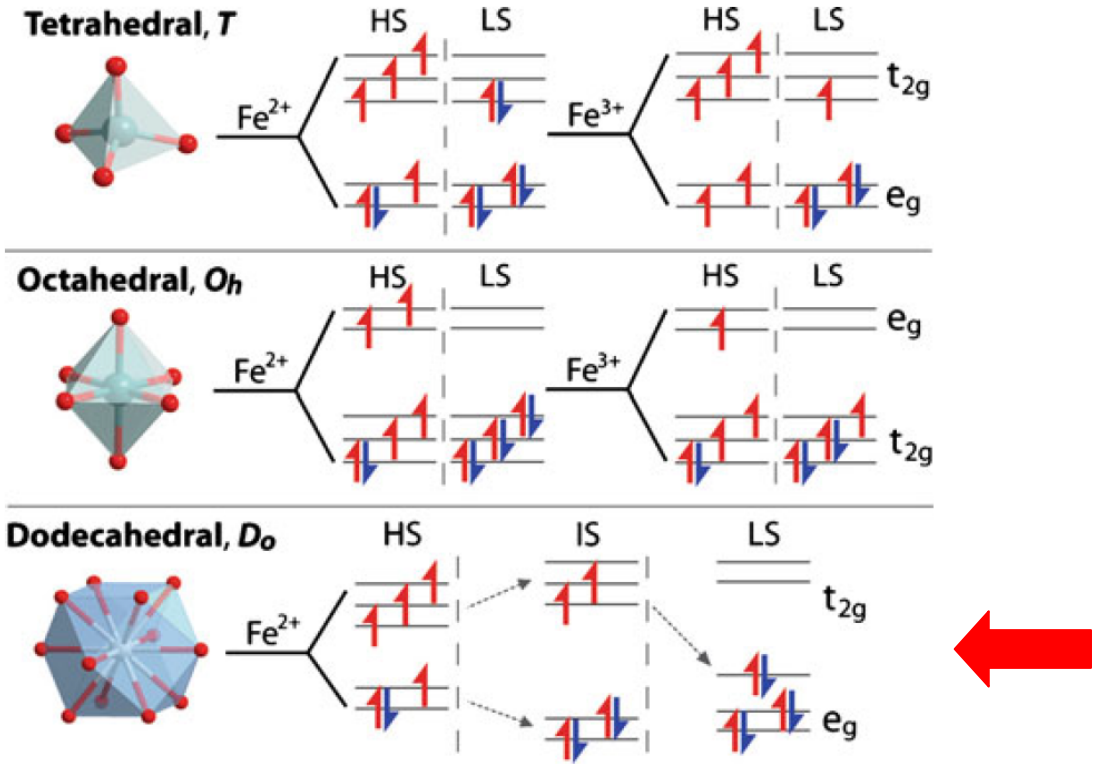

(Mg,Fe)SiO3:
HS → IS at 30 GPa
IS → LS at 120 GPa

Electronic spin state of iron in lower mantle perovskite

Jie Li*†, Viktor V. Struzhkin*, Ho-kwang Mao*, Jinfu Shu*, Russell J. Hemley*, Yingwei Fei*, Bjorn Mysen*, Przemek Dera*, Vitali Prakapenka‡, and Guoyin Shen‡

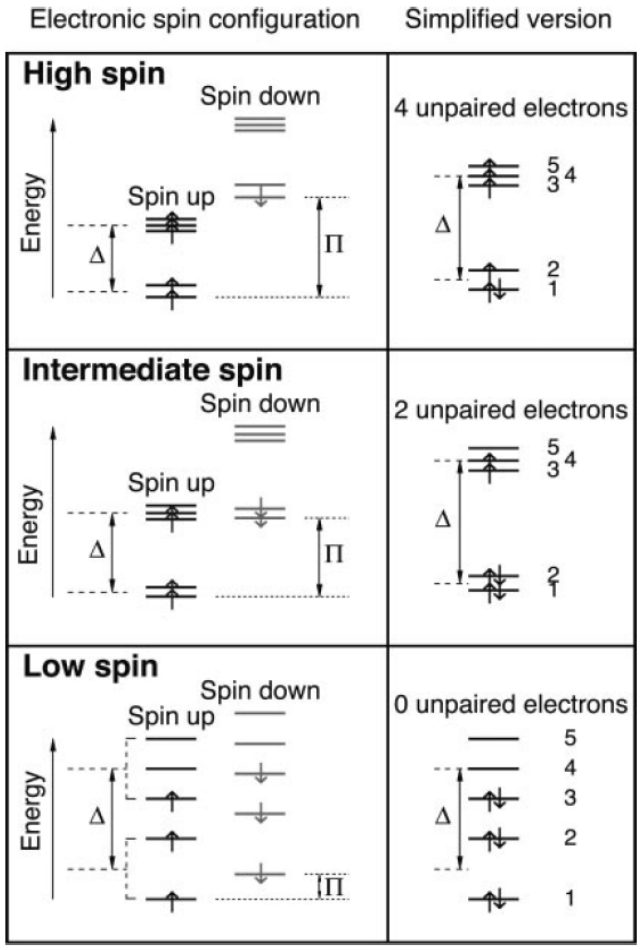

Fig. 4. Schematic diagrams of electronic spin configuration of Fe^{2+} in the A site of perovskite based on crystal field theory (4). On the right are the simplified pictures that are commonly found in the literature. The 3d subshell of iron contains five orbitals, each capable of accommodating two electrons with opposite spins. The energy difference between the opposite spins on each orbital (dotted lines) is called spin-pairing energy (*Π*). According to the crystal field theory, in a cubic environment, the 3d orbitals split into the t_{2g} and e_g levels (dashed lines). The energy difference between the two levels is called crystal field splitting energy (*Δ*). In a noncubic environment, additional splitting occurs between the t_{2g} levels and between the e_g levels, resulting in five different energy levels. At ambient condition, the 1st spin-down level is higher than the 5th spin-up level. Only one electron is forced to pair. Fe^{2+} has the largest number of unpaired electrons (high-spin state). Upon compression, crystal field splitting energy increases with increasing density (decreasing ligand bond lengths) and possibly increasing degree of distortion. Given fixed spin-pairing energy (5), certain lower spin-down levels will cross higher spin-up levels. When the 2nd spin-down level crosses the 5th spin-up level, the electron at the 5th orbital will switch spin and move to the 2nd orbital (intermediate-spin state, intermediate number of unpaired electrons). When the 3rd spin-down level crosses the 4th spin-up level, the electron at the 4th orbital will switch spin and move to the 3rd orbital (low-spin state, smallest number of unpaired electrons). In other words, each iron species goes through two pressure-induced partial spin-pairing transitions: Upon the first partial spin-pairing transition the number of unpaired 3d electrons drops to two, forming the intermediate-spin state. After the second partial transition, the number becomes zero, reaching the final low-spin state. Similar diagrams can be drawn for Fe^{3+} in either the A or the B site.

Iron spin transition in Earth's mantle

S. Speziale, A. Milner, V. E. Lee, S. M. Clark, M. P. Pasternak, and R. Jeanloz

High-pressure Mössbauer spectroscopy on several compositions across the (Mg,Fe)O magnesiowüstite solid solution confirms that ferrous iron (Fe^{2+}) undergoes a high-spin to low-spin transition at pressures and for compositions relevant to the bulk of the Earth's mantle. High-resolution x-ray diffraction measurements document a volume change of 4–5% across the pressure-induced spin transition, which is thus expected to cause seismological anomalies in the lower mantle. The spin transition can lead to dissociation of Fe-bearing phases such as magnesiowüstite, and it reveals an unexpected richness in mineral properties and phase equilibria for the Earth's deep interior.

17918–17922 | PNAS | December 13, 2005 | vol. 102 | no. 50

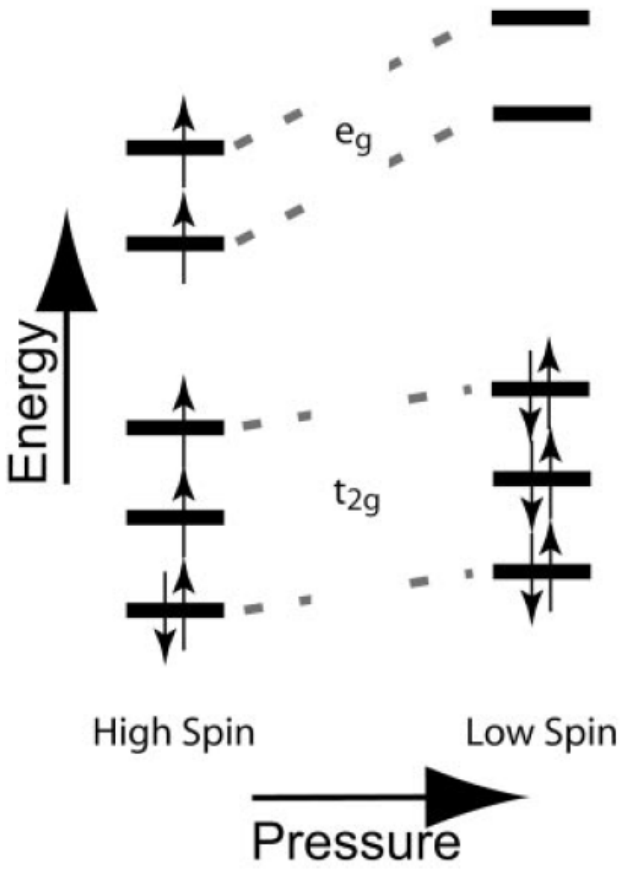

Spin Transition Zone in Earth's Lower Mantle

Jung-Fu Lin,[1] György Vankó,[2,3] Steven D. Jacobsen,[4] Valentin Iota,[1] Viktor V. Struzhkin,[5] Vitali B. Prakapenka,[6] Alexei Kuznetsov,[6] Choong-Shik Yoo[1]*

Mineral properties in Earth's lower mantle are affected by iron electronic states, but representative pressures and temperatures have not yet been probed. Spin states of iron in lower-mantle ferropericlase have been measured up to 95 gigapascals and 2000 kelvin with x-ray emission in a laser-heated diamond cell. A gradual spin transition of iron occurs over a pressure-temperature range extending from about 1000 kilometers in depth and 1900 kelvin to 2200 kilometers and 2300 kelvin in the lower mantle. Because low-spin ferropericlase exhibits higher density and faster sound velocities relative to the high-spin ferropericlase, the observed increase in low-spin (Mg,Fe)O at mid-lower mantle conditions would manifest seismically as a lower-mantle spin transition zone characterized by a steeper-than-normal density gradient.

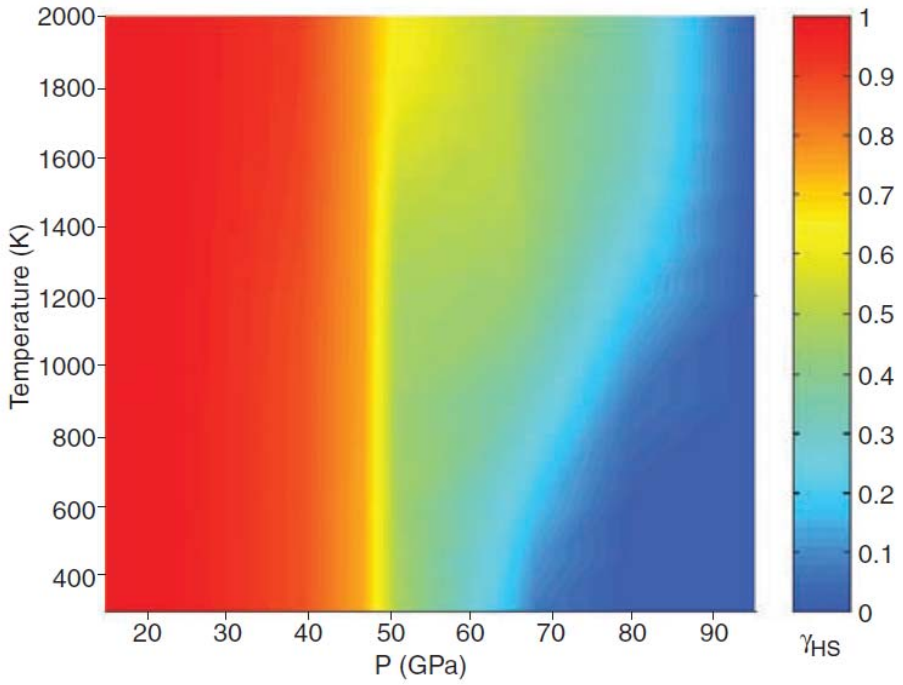

Fig. 3. Isosymmetric spin crossover of Fe^{2+} in $(Mg_{0.75}, Fe_{0.25})O$. The phase diagram is constructed from the interpolation and extrapolation of the derived fractions of the high-spin state in the sample (fig. S2). Colors in the vertical column on the right represent fractions of the high-spin iron, γ_{HS}, in $(Mg_{0.75},Fe_{0.25})O$.

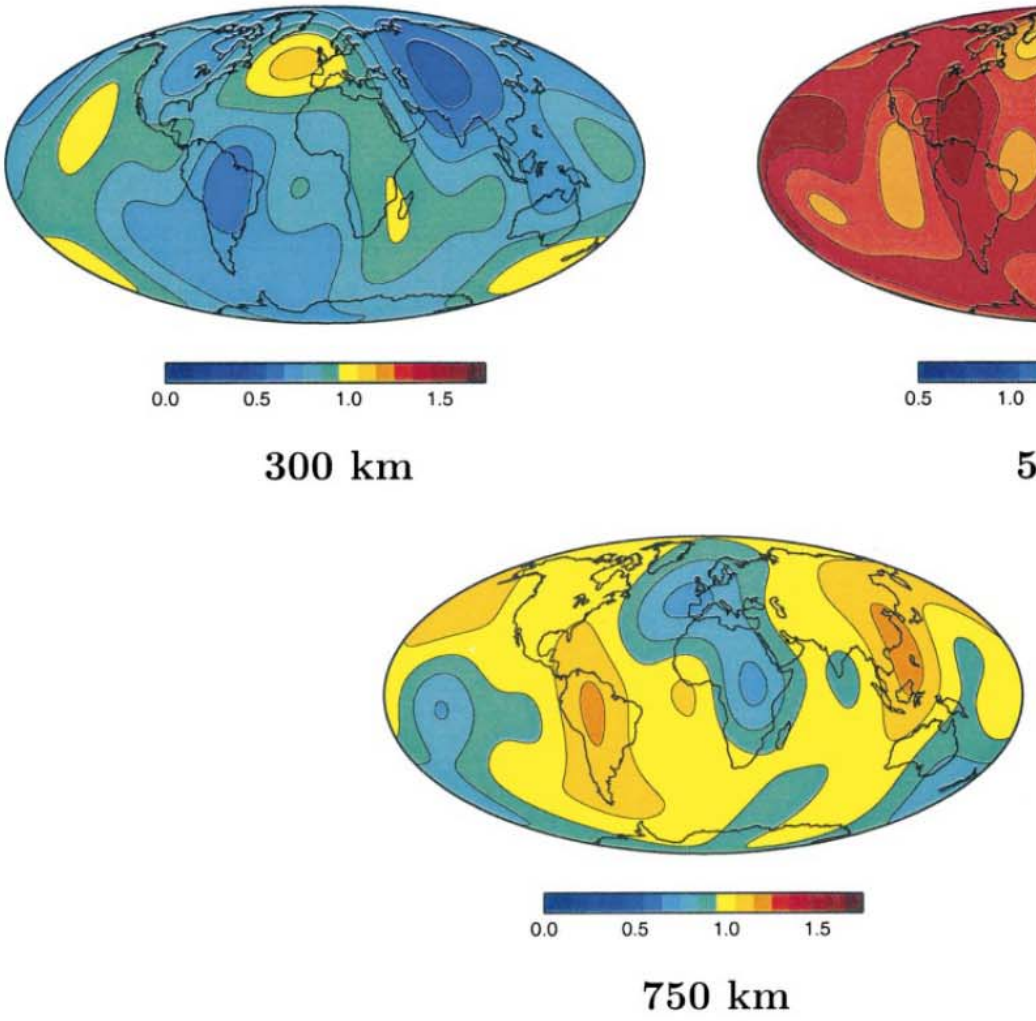

Fig. 7. Local Bullen's parameter η at the depths of 300, 500 and 750 km obtained from the 3-D model of density and seismic velocities published by Ishii and Tromp [12].

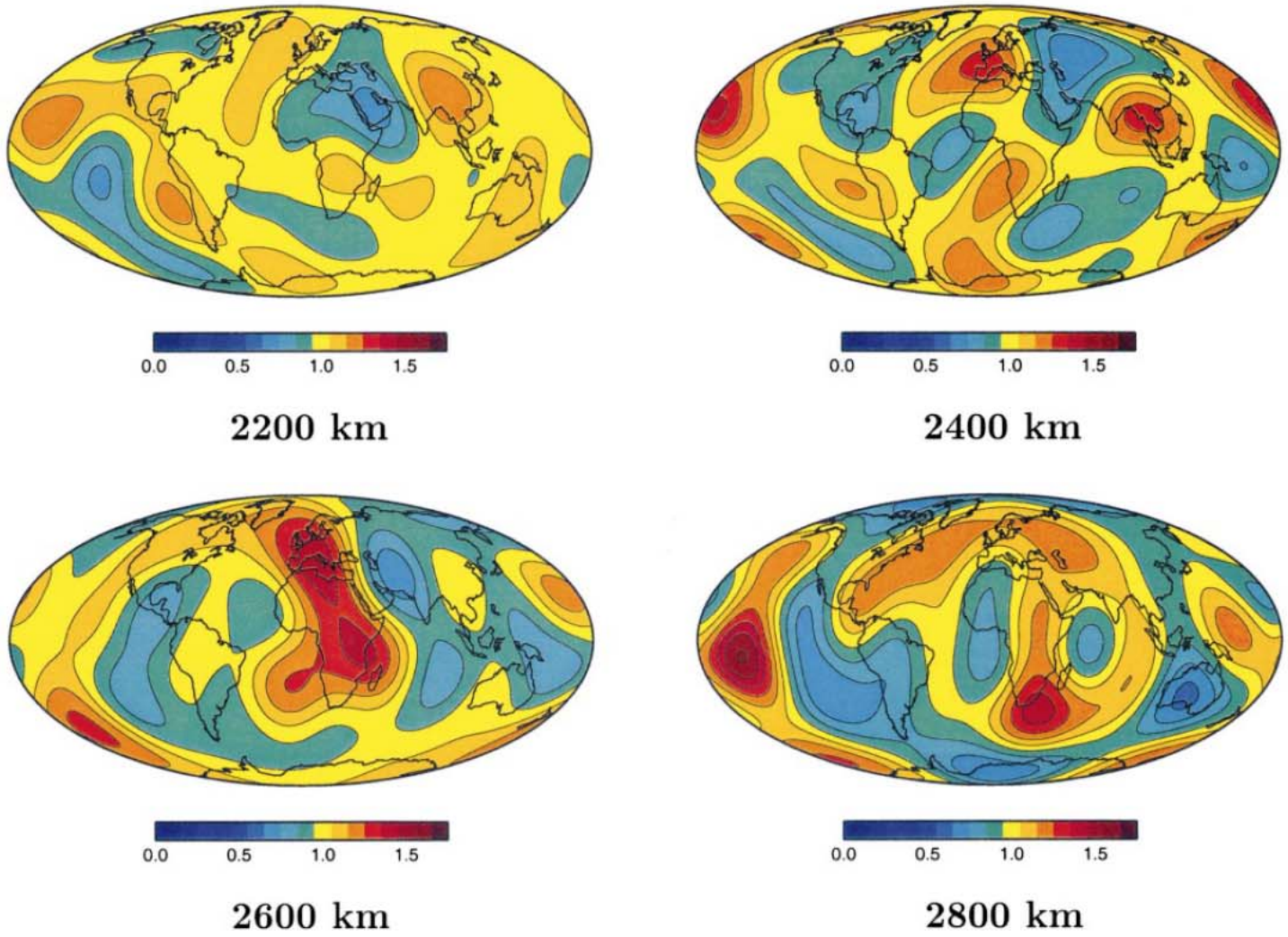

Fig. 6. Local Bullen's parameter η at the four depths in the lower part of the lower mantle – 2200, 2400, 2600 and 2800 km – obtained from the 3-D model of density and seismic velocities published by Ishii and Tromp [12].

Available online at www.sciencedirect.com
ScienceDirect
Physics of the Earth and Planetary Interiors 170 (2008) 248–259
PHYSICS OF THE EARTH AND PLANETARY INTERIORS
www.elsevier.com/locate/pepi

Spin transition of iron in the Earth's lower mantle

Jung-Fu Lin [a,*], Taku Tsuchiya [b]

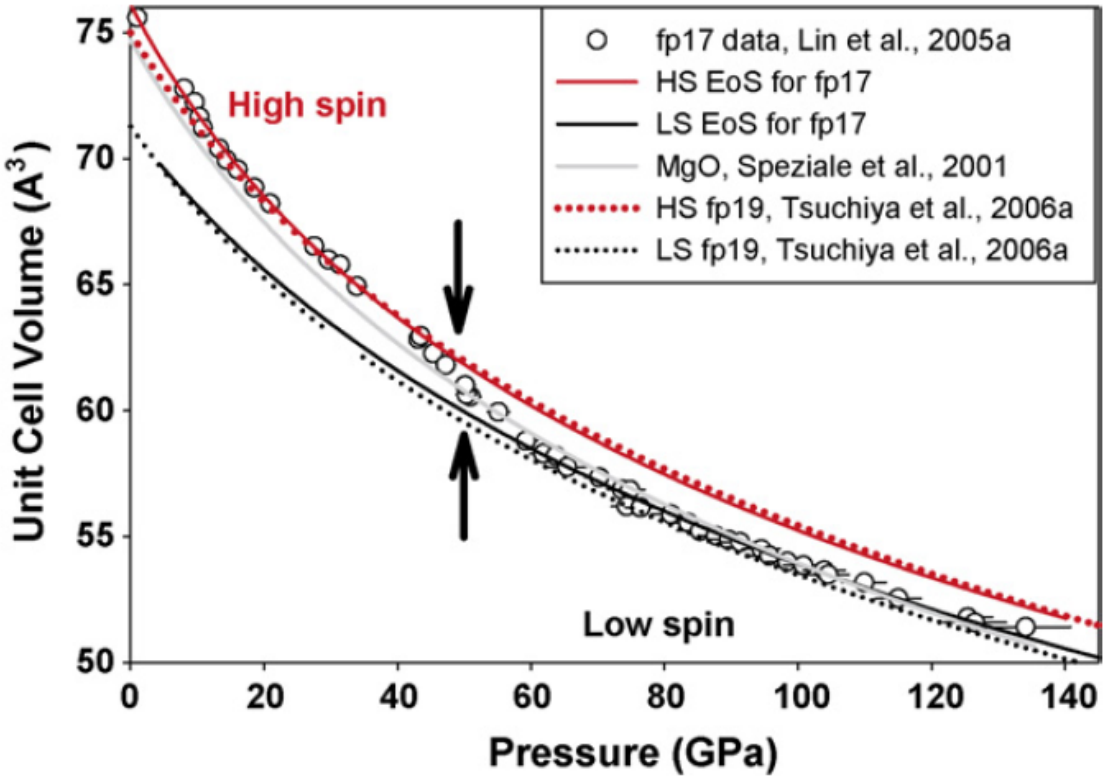

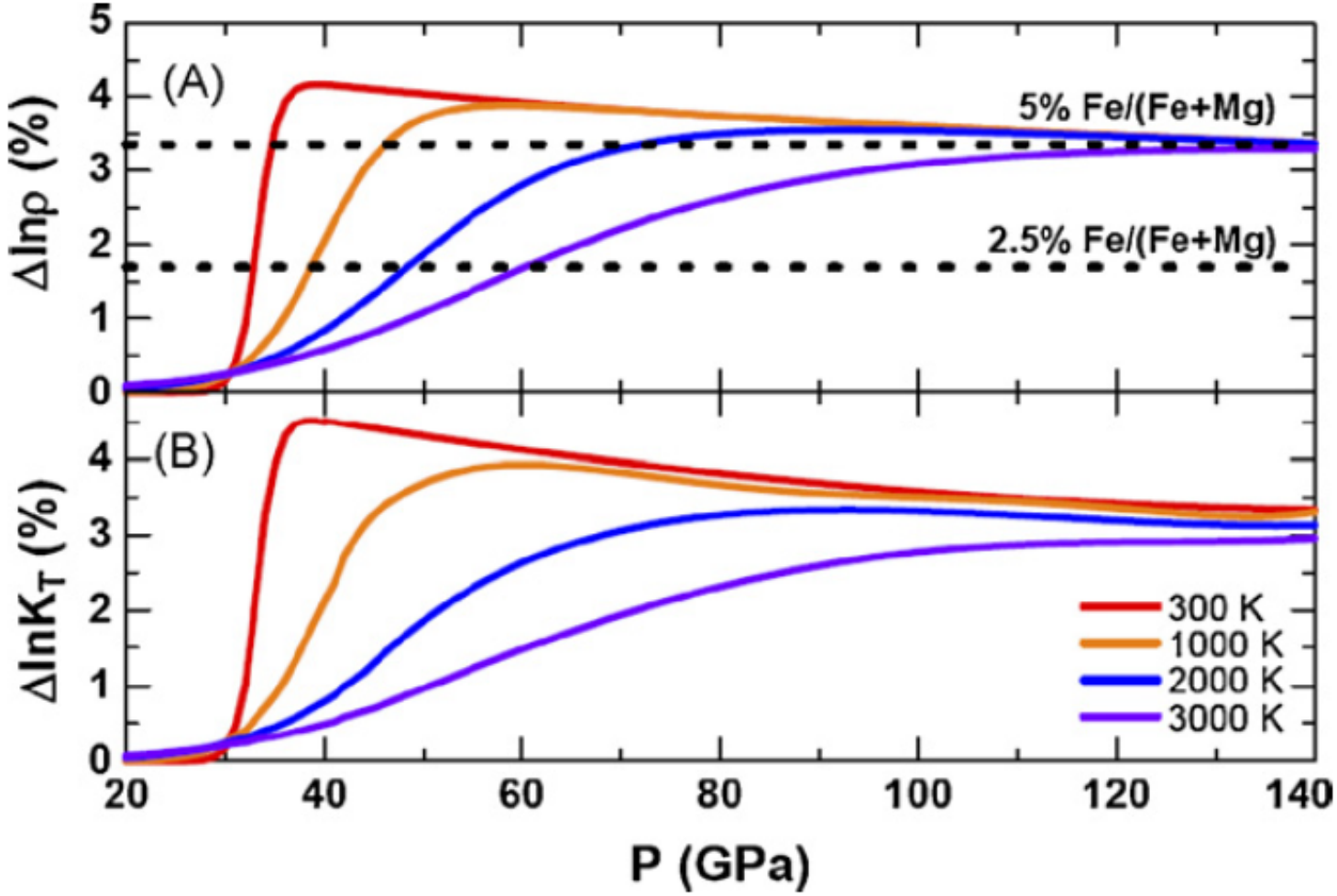

Fig. 9. Calculated density (A) and bulk modulus (B) variations in percentage for ($Mg_{0.8125}$,$Fe_{0.1875}$)O) as derived from Fig. 8.

Spin Crossover in Ferropericlase at High Pressure: A Seismologically Transparent Transition?

Daniele Antonangeli,[1,2]* Julien Siebert,[1,2] Chantel M. Aracne,[2] Daniel L. Farber,[2,3] A. Bosak,[4] M. Hoesch,[4] M. Krisch,[4] Frederick J. Ryerson,[2] Guillaume Fiquet,[1] James Badro[1,2]

Seismic discontinuities in Earth typically arise from structural, chemical, or temperature variations with increasing depth. The pressure-induced iron spin state transition in the lower mantle may influence seismic wave velocities by changing the elasticity of iron-bearing minerals, but no seismological evidence of an anomaly exists. Inelastic x-ray scattering measurements on $(Mg_{0.83}Fe_{0.17})O$-ferropericlase at pressures across the spin transition show effects limited to the only shear moduli of the elastic tensor. This explains the absence of deviation in the aggregate seismic velocities and, thus, the lack of a one-dimensional seismic signature of the spin crossover. The spin state transition does, however, influence shear anisotropy of ferropericlase and should contribute to the seismic shear wave anisotropy of the lower mantle.

7 JANUARY 2011 VOL 331 **SCIENCE**

Elastic Shear Anisotropy of Ferropericlase in Earth's Lower Mantle

Hauke Marquardt,[1]* Sergio Speziale,[1] Hans J. Reichmann,[1] Daniel J. Frost,[2] Frank R. Schilling,[1]† Edward J. Garnero[3]

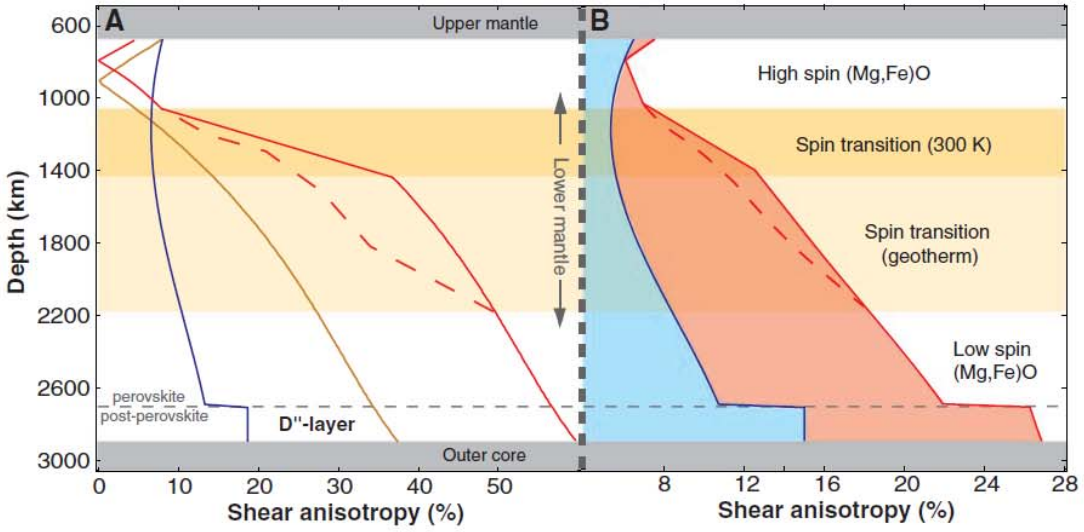

Fig. 4. Maximum shear anisotropy of major lower-mantle phases along a model geotherm. The shear polarization anisotropy is defined as $(v_{s,max} - v_{s,min})/[(v_{s,max} + v_{s,min})/2]$, where $v_{s,max}$ and $v_{s,min}$ are maximum and minimum shear velocity in a given direction. (**A**) The maximum single-crystal polarization anisotropy of the two major components of Earth's lower mantle. The shear anisotropy of MgO (gold) and $MgSiO_3$ (blue) were calculated with available computational data at high pressure and temperature. The elastic anisotropy of $(Mg_{0.8}Fe_{0.2})O$ (red), a model mantle composition, was linearly scaled from the data of MgO and $(Mg_{0.9}Fe_{0.1})O$, corrected for temperature (*24*). The expected broadening of the spin transition region (dashed lines) with temperature was estimated from experimental data on $(Mg_{0.75}Fe_{0.25})O$ (*33*). (**B**) The anisotropies of the single phases were weighted by their volume abundance in the lower mantle (*24*), where the shaded areas illustrate the maximum possible contributions of perovskite (blue) and ferropericlase (red), a situation in which all the crystals of the same mineral phase have the same orientation.

Is the spin transition in Fe^{2+}-bearing perovskite visible in seismology?

Razvan Caracas,[1] David Mainprice,[2] and Christine Thomas[3]

[1] We determine the elasticity of $FeSiO_3$ perovskite for various spin configurations using density-functional theory calculations. The elastic moduli and the bulk seismic wave velocities are weakly affected by the spin transition. However we show that the intrinsic differences in seismic anisotropy between the high-spin and low-spin phases of Fe-bearing perovskite coupled with lattice preferred orientation that can develop due and during the convection may lead to distinct seismic signatures between the top and the bottom of the lower mantle. These signatures should be detectable in observations and they need to be taken into account in tomographic studies of the Earth's lower mantle. **Citation:** Caracas, R., D. Mainprice, and C. Thomas (2010), Is the spin transition in Fe^{2+}-bearing perovskite visible in seismology?, *Geophys. Res. Lett.*, *37*, L13309, doi:10.1029/2010GL043320.

RADIATIVE THERMAL CONDUCTIVITY

For the Earth's mantle thermal conductivity k (T, P, d, Fe…) has two principal components:

- k-lattice, phonons.
- k-radiative, the important player in mantle dynamics. It goes like T^3 and other powers of T (T^2 and T), it depends on water content and grain-size (*Hofmeister 2005, Journal of Geodynamics).*

Recently, the discovery of spin-pairing in mantle minerals under high pressure has led to a renewed interest in radiative conductivity, because spin-pairing could potentially change optical absorption spectra drastically and it may therefore have a strong effect on radiative heat transport. At the same time, recent optical absorption measurements at high pressures suggested that iron-bearing mantle minerals do not necessarily become opaque at high pressures *(Keppler et al. 2008, Science).*

RADIATIVE THERMAL CONDUCTIVITY

Electronic Transitions in Perovskite: Possible Nonconvecting Layers in the Lower Mantle

James Badro,[1]* Jean-Pascal Rueff,[2] György Vankó,[3]
Giulio Monaco,[3] Guillaume Fiquet,[1] François Guyot[1]

We measured the spin state of iron in magnesium silicate perovskite $(Mg_{0.9},Fe_{0.1})SiO_3$ at high pressure and found two electronic transitions occurring at 70 gigapascals and at 120 gigapascals, corresponding to partial and full electron pairing in iron, respectively. The proportion of iron in the low spin state thus grows with depth, increasing the transparency of the mantle in the infrared region, with a maximum at pressures consistent with the D″ layer above the core-mantle boundary. The resulting increase in radiative thermal conductivity suggests the existence of nonconvecting layers in the lowermost mantle.

[1]Laboratoire de Minéralogie Cristallographie de Paris (UMR CNRS 7590), Institut de Physique du Globe de Paris, Université Paris, 6 and 7, 4 Place Jussieu, 75252 Paris, France. [2]Laboratoire de Chimie Physique–Matière et Rayonnement (UMR CNRS 7614), Université Paris, 6 11 Rue Pierre et Marie Curie, 75231 Paris, France. [3]European Synchrotron Radiation Facility (ESRF), B.P. 220 F-38043 Grenoble CEDEX, France

RADIATIVE THERMAL CONDUCTIVITY

Electronic spin state of iron in lower mantle perovskite

Jie Li*†, Viktor V. Struzhkin*, Ho-kwang Mao*, Jinfu Shu*, Russell J. Hemley*, Yingwei Fei*, Bjorn Mysen*, Przemek Dera*, Vitali Prakapenka‡, and Guoyin Shen‡

*Geophysical Laboratory, Carnegie Institution of Washington, 5251 Broad Branch Road NW, Washington, DC 20015; and ‡Consortium for Advanced Radiation Sources, University of Chicago, 9700 South Cass Avenue, Argonne, IL 60439

Contributed by Ho-kwang Mao, August 16, 2004

Furthermore, it has been proposed that the high-spin Fe^{2+} ions in the lower mantle perovskite may hinder the blackbody radiation in near-infrared regions. The presence of low-spin Fe^{2+} ions in perovskite would confine the crystal field transitions to the visible region, hence allowing more efficient radiative heat transfer at near-infrared wavelengths in the deep mantle (4). Possible chemical stratifi-

RADIATIVE THERMAL CONDUCTIVITY

Optical Absorption and Radiative Thermal Conductivity of Silicate Perovskite to 125 Gigapascals

Hans Keppler,[1]* Leonid S. Dubrovinsky,[1] Olga Narygina,[1] Innokenty Kantor[1,2]

[1]Bayerisches Geoinstitut, Universität Bayreuth, 95440 Bayreuth, Germany. [2]Advanced Photon Source, Argonne National Laboratory, Argonne, IL 60439, USA.

Mantle convection and plate tectonics are driven by the heat flow from Earth's core to the surface. The radiative contribution to heat transport is usually assumed to be negligible. Here, we report the near-infrared and optical absorption spectra of silicate perovskite, the main constituent of the lower mantle, to 125 gigapascals. Silicate perovskite remains quite transparent up to the pressures at the core-mantle boundary. Estimates of radiative thermal conductivity derived from these spectra approach 10 watts meter^{-1} kelvin^{-1} at lowermost mantle conditions, implying that heat conduction is dominated by radiation. However, the increase in radiative conductivity with temperature (T) is less pronounced than expected from a T^3 dependency.

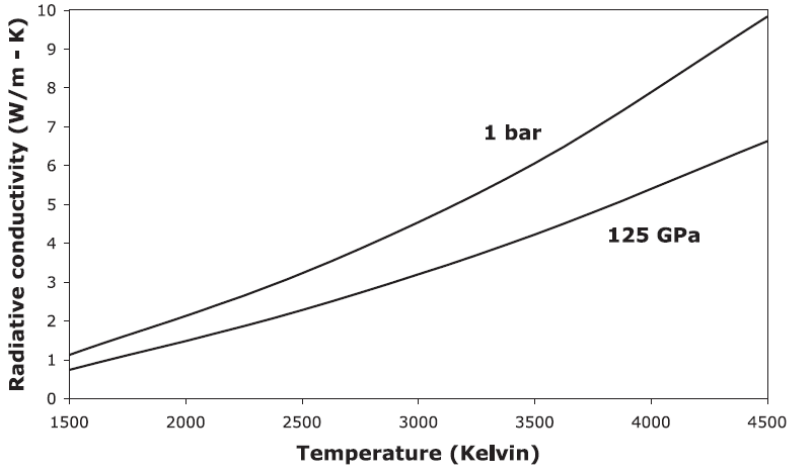

Fig. 3. Estimated radiative thermal conductivity of silicate perovskite as a function of temperature. Calculations have their bases in the 125-GPa spectrum and the 1-bar spectrum in Fig. 1. The 125-GPa data contain a correction for the increase of the optical absorption coefficient that results from the reduction of sample thickness by about 9% upon compression, calculated with K = 261 GPa and K' = 4.1 (*25*). At high temperatures, the intervalence charge transfer band seen in the 125-GPa spectrum may disappear, and therefore the calculation based on the 1-bar spectrum may actually give more accurate values for the radiative thermal conductivity in the lower mantle. Whereas temperatures at the core mantle boundary are between 3300 and 4300 K, mantle temperatures at 125 GPa (2770 km depth) may reach 3000 to 3500 K (*26*).

RADIATIVE THERMAL CONDUCTIVITY

Reduced Radiative Conductivity of Low-Spin (Mg,Fe)O in the Lower Mantle

Alexander F. Goncharov,* Viktor V. Struzhkin, Steven D. Jacobsen†

Optical absorption spectra have been measured at pressures up to 80 gigapascals (GPa) for the lower-mantle oxide magnesiowüstite (Mg,Fe)O. Upon reaching the high-spin to low-spin transition of Fe^{2+} at about 60 GPa, we observed enhanced absorption in the mid- and near-infrared spectral range, whereas absorption in the visible-ultraviolet was reduced. The observed changes in absorption are in contrast to prediction and are attributed to *d-d* orbital charge transfer in the Fe^{2+} ion. The results indicate that low-spin (Mg,Fe)O will exhibit lower radiative thermal conductivity than high-spin (Mg,Fe)O, which needs to be considered in future geodynamic models of convection and plume stabilization in the lower mantle.

Geophysical Laboratory, Carnegie Institution of Washington, 5251 Broad Branch Road, NW, Washington, DC

RADIATIVE THERMAL CONDUCTIVITY

Spin-paired Iron in Ultra-low Velocity Zones

Wendy L. Mao[1,2], Ho-kwang Mao[1,2,3], Michael Hu[3], Paul Chow[3], Yue Meng[3], Guoyin Shen[4], Vitali B. Prakapenka[4], Jinfu Shu[2], Andrew J. Campbell[5], Yingwei Fei[2], and Russell J. Hemley[2]

The boundary layer between the crystalline, silicate mantle and the liquid, Fe-alloy outer core contains regions with ultra-low seismic velocities. In experiments simulating the high pressure-temperature conditions of the core-mantle boundary, we observed that the magnetic, spin-parallel, electronic state of Fe collapsed into a spin-paired state when Fe entered the post-perovskite silicate phase. The spin-paired electronic state reduces the free energy of formation, reduces the Fe partial molar volume, reduces the seismic velocity, increases Fe partitioning in the silicate, and reduces infrared absorption. It would enable the mantle silicate to uptake Fe from the metallic core to form a dense, Fe-rich silicate layer, offering a possible explanation for the observed ultra-low velocity zones.

submitted to Science ??, 2005 ??

Iron-Rich Post-Perovskite and the Origin of Ultralow-Velocity Zones

Wendy L. Mao,[1*] Ho-kwang Mao,[2,3] Wolfgang Sturhahn,[4] Jiyong Zhao,[4] Vitali B. Prakapenka,[5] Yue Meng,[3] Jinfu Shu,[2] Yingwei Fei,[2] Russell J. Hemley[2]

The boundary layer between the crystalline silicate lower mantle and the liquid iron core contains regions with ultralow seismic velocities. Such low compressional and shear wave velocities and high Poisson's ratio are also observed experimentally in post-perovskite silicate phase containing up to 40 mol% $FeSiO_3$ endmember. The iron-rich post-perovskite silicate is stable at the pressure-temperature and chemical environment of the core-mantle boundary and can be formed by core-mantle reaction. Mantle dynamics may lead to further accumulation of this material into the ultralow-velocity patches that are observable by seismology.

28 APRIL 2006 VOL 312 **SCIENCE**

RADIATIVE THERMAL CONDUCTIVITY

ELSEVIER

Available online at www.sciencedirect.com

ScienceDirect

Earth and Planetary Science Letters 249 (2006) 436–443

EPSL

www.elsevier.com/locate/epsl

Valence state and spin transitions of iron in Earth's mantle silicates

Feiwu Zhang *, Artem R. Oganov

Our results imply that at mantle conditions *PPv* should have lower radiative conductivity than *Pv* and, therefore, it is unlikely that radiative conductivity can stabilize the D" layer against convection. The D" layer could, nevertheless, be nonconvecting if it is sufficiently compositionally different from the rest of the lower mantle.

RADIATIVE THERMAL CONDUCTIVITY

Intermediate-spin ferrous iron in lowermost mantle post-perovskite and perovskite

JUNG-FU LIN[1]*, HEATHER WATSON[2], GYÖRGY VANKÓ[3], ESEN E. ALP[4], VITALI B. PRAKAPENKA[5], PRZEMEK DERA[5], VIKTOR V. STRUZHKIN[6], ATSUSHI KUBO[5], JIYONG ZHAO[4], CATHERINE McCAMMON[7] AND WILLIAM J. EVANS[2]

Our studies show that both perovskite and post-perovskite accommodate the same intermediate-spin Fe^{2+} and that their opacity and absorption behaviour in the infrared wavelength range are very similar in our high pressure–temperature experiments. These indicate that corresponding changes in the radiative thermal conductivity, electrical conductivity and iron partitioning would be due to the crystal structural transition, rather than the electronic spin transition, from perovskite to post-perovskite; although, the spin state of Fe^{3+} and its effects in these phases remain to be understood.

nature geoscience | VOL 1 | OCTOBER 2008 |

Physics of the Earth and Planetary Interiors 180 (2010) 215–221

Contents lists available at ScienceDirect

Physics of the Earth and Planetary Interiors

journal homepage: www.elsevier.com/locate/pepi

Low-spin Fe^{2+} in silicate perovskite and a possible layer at the base of the lower mantle

C. McCammon[a,*], L. Dubrovinsky[a], O. Narygina[a], I. Kantor[a,1], X. Wu[a], K. Glazyrin[a], I. Sergueev[b], A.I. Chumakov[b]

[a] Bayerisches Geoinstitut, Universität Bayreuth, D-95440 Bayreuth, Germany
[b] European Synchrotron Radiation Facility, BP 220, F-38043 Grenoble Cedex, France

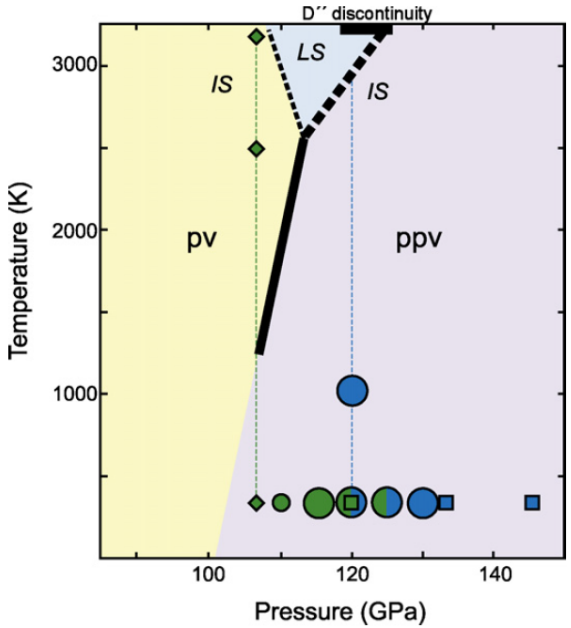

Fig. 7. Proposed phase boundary for $(Mg,Fe)(Si,Al)O_3$ between perovskite (pv) and post-perovskite (ppv). The thick solid line indicates the phase boundary summarised from data in the literature (Hirose, 2006), which may be shifted to higher pressures due to an intermediate-spin (IS) to low-spin (LS) transition in the perovskite phase, creating a region where silicate perovskite containing low-spin Fe^{2+} is stable (blue). The region where IS Fe^{2+} is stable in the perovskite structure is shaded yellow, while the region where IS Fe^{2+} is stable in the post-perovskite structure is shaded purple. Symbols indicate the spin state determined for Fe^{2+} in silicate perovskite, where green indicates intermediate-spin and blue indicates low-spin: large circles (this work); small circle (McCammon et al., 2008); diamonds (Lin et al., 2008); squares (Badro et al., 2004). The estimated depth range of the D″ discontinuity is indicated by the black bar (e.g., Wysession et al., 1998), and the green and blue dashed lines are a guide for the eye.

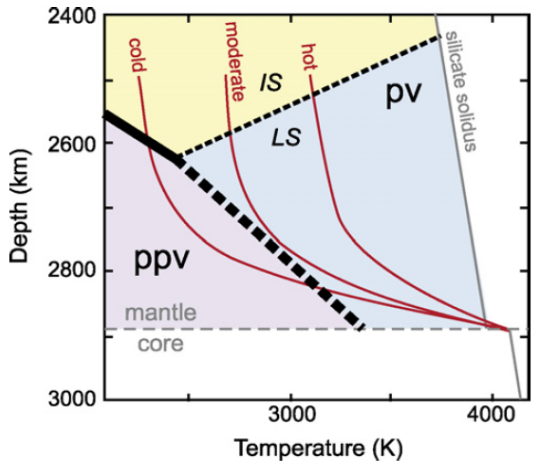

Fig. 8. The estimated thermal structure of D″ adapted from Hernlund et al. (2005). The perovksite to post-perovksite transition is shown by the thick solid (existing data) and dashed (our proposed boundary) lines, and various geotherms are shown in red. The region where IS Fe^{2+} is stable in the perovskite structure is shaded yellow, while the region where IS Fe^{2+} is stable in the post-perovskite structure is shaded purple. The blue region is where silicate perovskite containing low-spin Fe^{2+} would be stable, which leads to the presence of post-perovskite lenses in cold regions (as already proposed by Hernlund et al., 2005), but with intermediate-spin Fe^{2+} silicate perovskite above and low-spin Fe^{2+} silicate perovskite below. (For interpretation of the references to color in this figure legend, the reader is referred to the web version of the article.)

Anomalous thermodynamic properties in ferropericlase throughout its spin crossover

Z. Wu (吴忠庆),[1] J. F. Justo,[1,2] C. R. S. da Silva,[3] S. de Gironcoli,[4,5] and R. M. Wentzcovitch[1,3]

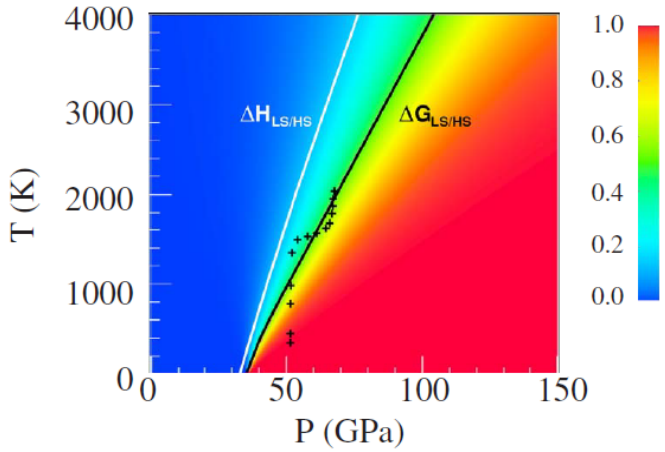

FIG. 5. (Color online) "Phase diagram" of Fp with $x=0.1875$. The black and white lines correspond to the middle point of the crossover, where $n(P,T)=0.5$, computed with and without including the vibrational contribution to the free energy, respectively. The plus symbols are experimental data corresponding to $n=0.5$ (Ref. 9).

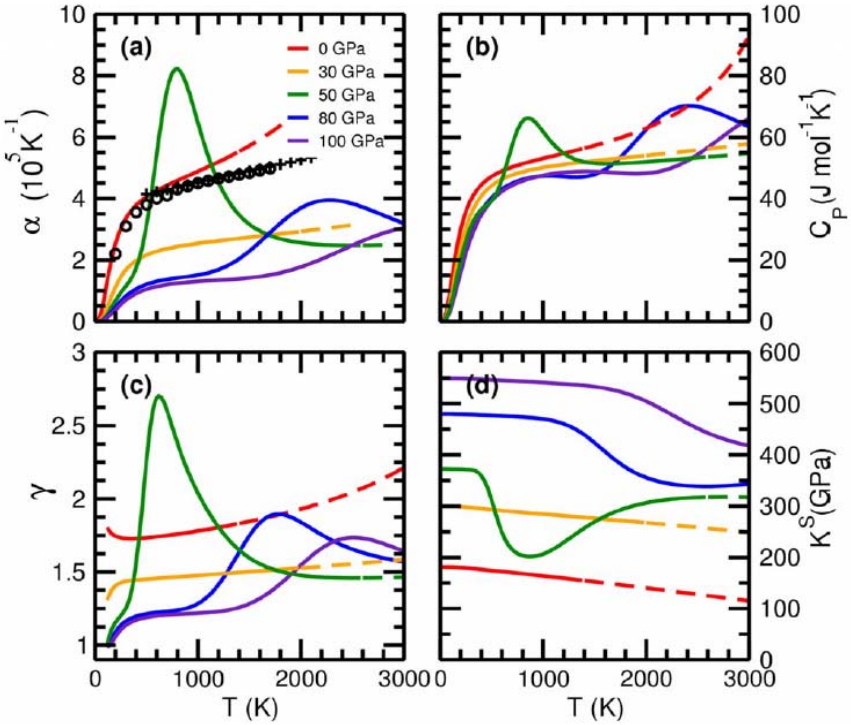

FIG. 7. (Color online) Thermodynamics properties of Fp as a function of temperature along several isobars. The figure presents (a) thermal-expansion coefficient, (b) heat capacity at constant pressure, (c) thermal Grüneisen parameter, and (d) adiabatic bulk modulus. Full (dashed) lines correspond to results within (outside) the PT regime of validity of the QHA. Circles and crosses in (a) are experimental thermal expansivities at 0 GPa for $Mg_{1-x}Fe_xO$, respectively, with $x=0.0$ (Ref. 38) and with $x=0.36$ (Ref. 31).

MANTLE VISCOSITY

ELSEVIER

Available online at www.sciencedirect.com

SCIENCE DIRECT

Earth and Planetary Science Letters 225 (2004) 177–189

EPSL

www.elsevier.com/locate/epsl

A new inference of mantle viscosity based upon joint inversion of convection and glacial isostatic adjustment data

J.X. Mitrovica[a,*], A.M. Forte[b,1]

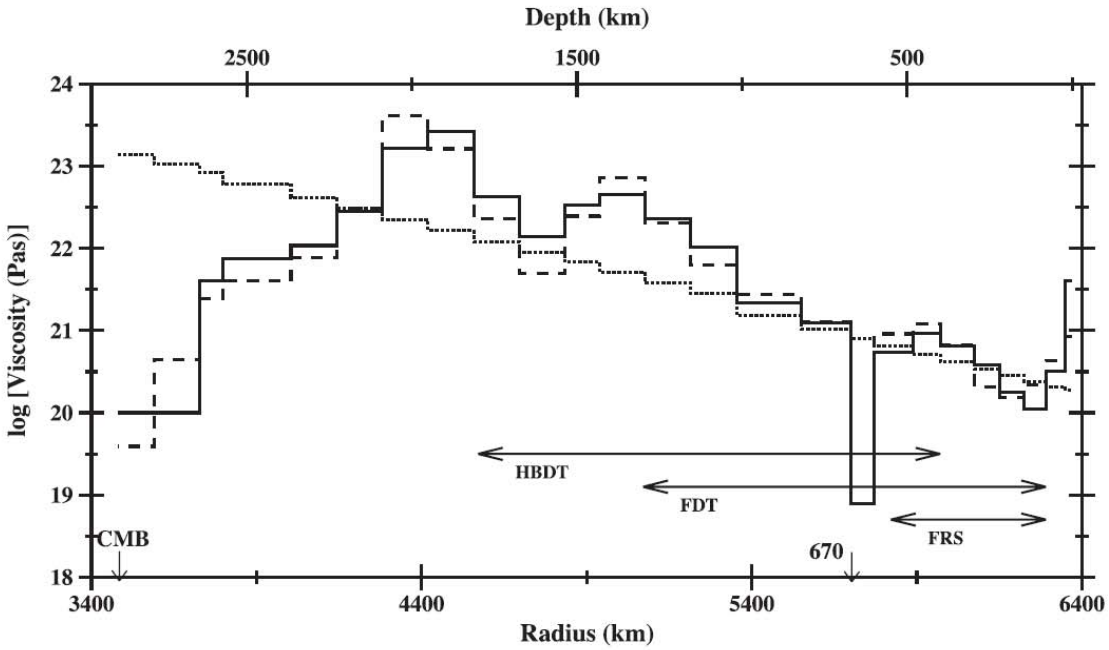

Fig. 3. Results of Occam-style inversions (see text for details) of the GIA and convection data sets described in the text. The dotted curve is the inference based on the inversion of GIA data alone. The solid and dashed lines are joint inversions of GIA and convection data sets distinguished on the basis of the seismic shear wave heterogeneity model adopted in the prediction of convection observables (Grand [54] and Ekström and Dziewonski [55], respectively). The solid and dashed profiles have a viscosity value of 7.8×10^{18} Pa s in the low-viscosity layer above 670 km depth. The three horizontal solid lines represent three of the radial regions resolved by the GIA data, as estimated in previous studies (see text). These include constraints imposed by: the Fennoscandian decay time ("FDT"), Hudson Bay decay times ("HBDT") and the Fennoscandian relaxation spectrum ("FRS").

Ferrous iron diffusion in ferro-periclase across the spin transition

M.W. Ammann *, J.P. Brodholt, D.P. Dobson

EPSL, 2011

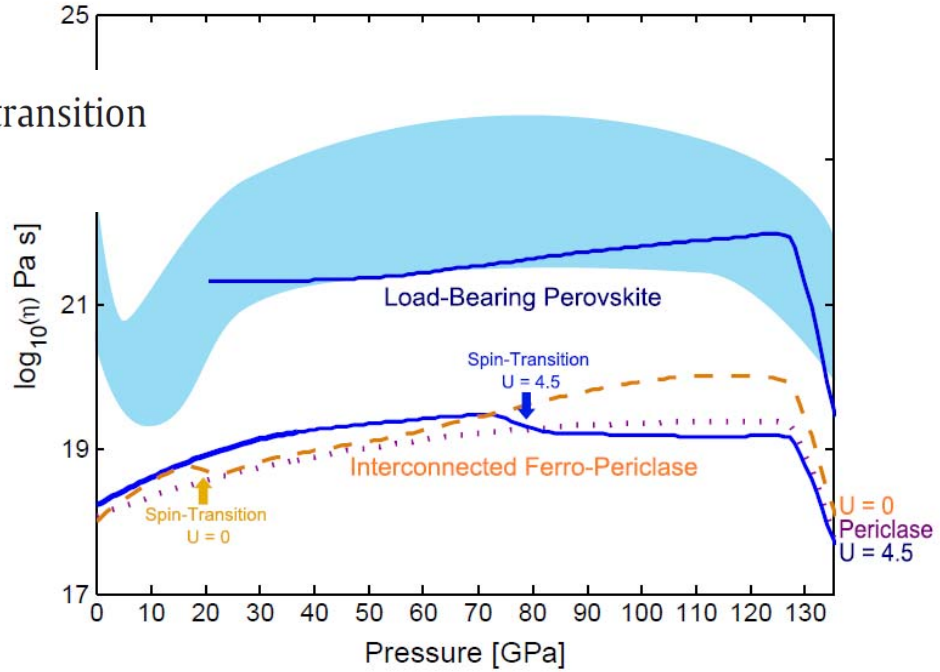

Fig. 9. Comparison of diffusion creep viscosities along a geotherm (Stacey and Davis, 2004) with the results from inversion modelling (light blue area; e.g. Forte and Mitrovica, 2001; Hager and Richards, 1989; Mitrovica and Forte, 2004; Peltier and Drummond, 2008; Ricard and Wuming, 1991; Steinberger and Calderwood, 2006). Parameters for ferro-periclase are either a grain size of $G = 1$ mm and a vacancy concentration of $N_v = 10^{-3}$ or a grain size of $G = 0.1$ mm and a vacancy concentration of $N_v = 10^{-5}$ (see text for details). The viscosity profile of perovskite is the same as in Ammann et al. (2010b). Vacancy concentrations for both minerals were assumed to be fixed throughout the entire lower mantle. Dashed (U = 0) and solid (U = 4.5) lines are the lower bounds where ferro-periclase forms an interconnected network, for the upper bound perovskite is the load-bearing phase of the two phase system (Takeda, 1998) (20% ferro-periclase, containing 20% or 0% (dotted line) iron, 80% perovskite). The small kinks, just after 20 GPa (U = 0) and around 75 GPa (U = 4.5) are a viscosity reduction due to the spin-transitions as indicated with arrows (initial kink: transition at th the W_1 saddle-point, final kink transition of the ground-state with vacancy on nearest neighbour site to iron). (For interpretation of the references to color in this figure legend, the reader is referred to the web version of this article.)

MANTLE VISCOSITY

$$\eta = A \exp\left(\frac{G^*}{RT^*}\right)$$

$$G^* = E^* + p^*V^*$$

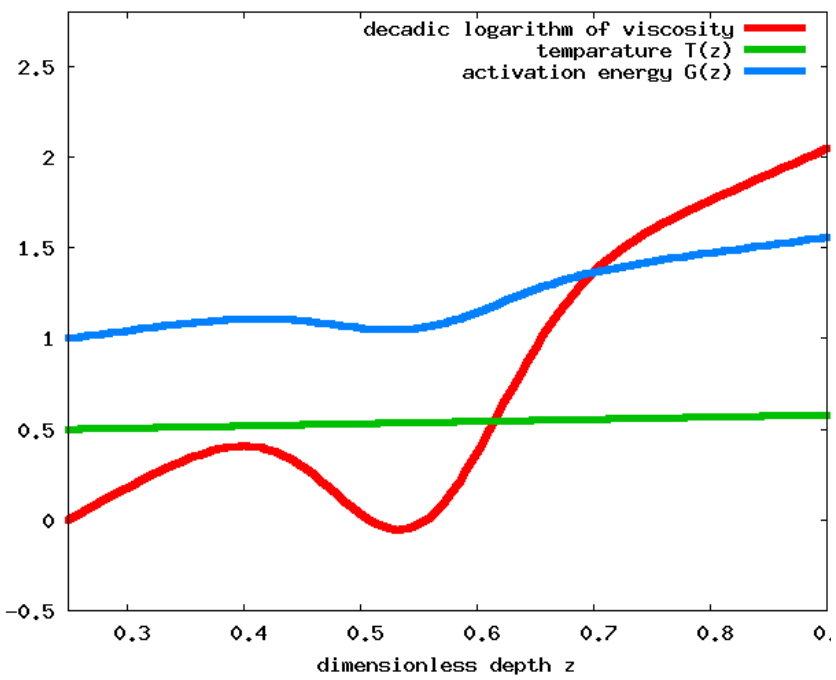

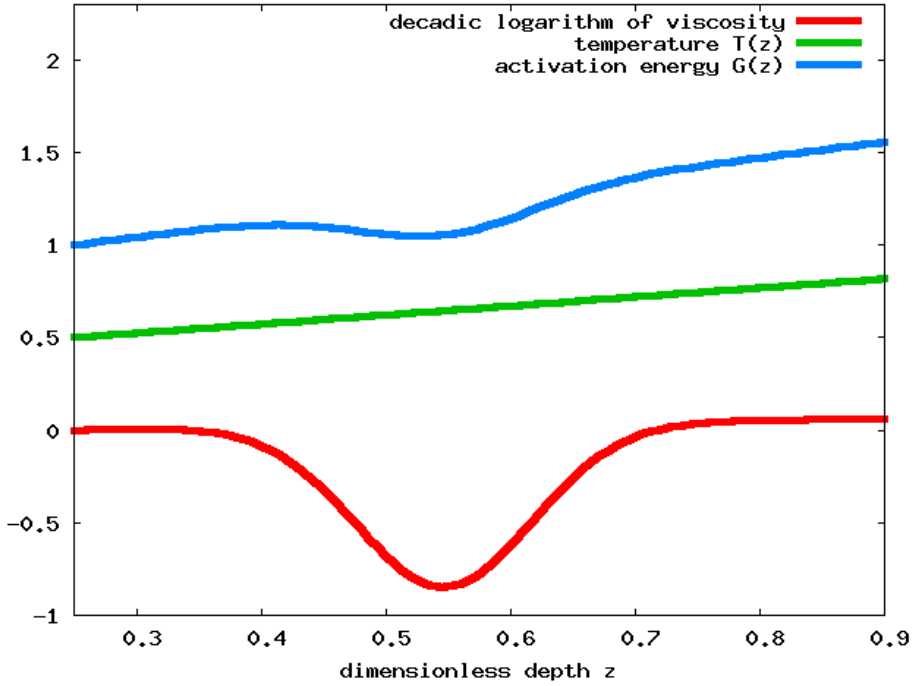

Anomalous compressibility of ferropericlase throughout the iron spin cross-over

R. M. Wentzcovitch[a,b,1], J. F. Justo[a,b,c], Z. Wu[a,b], C. R. S. da Silva[b], D. A. Yuen[b,d], and D. Kohlstedt[d]

The thermoelastic properties of ferropericlase $Mg_{1-x}Fe_xO$ (x = 0.1875) throughout the iron high-to-low spin cross-over have been investigated by first principles at Earth's lower mantle conditions. This cross-over has important consequences for elasticity such as an anomalous bulk modulus (K_S) reduction. At room temperature the anomaly is somewhat sharp in pressure but broadens with increasing temperature. Along a typical geotherm it occurs across most of the lower mantle with a more significant K_S reduction at ≈1,400–1,600 km depth. This anomaly might also cause a reduction in the effective activation energy for diffusion creep and lead to a viscosity minimum in the mid-lower mantle, in apparent agreement with results from inversion of data related with mantle convection and postglacial rebound.

Earth's lower mantle | viscosity | thermodynamics | thermal expansivity

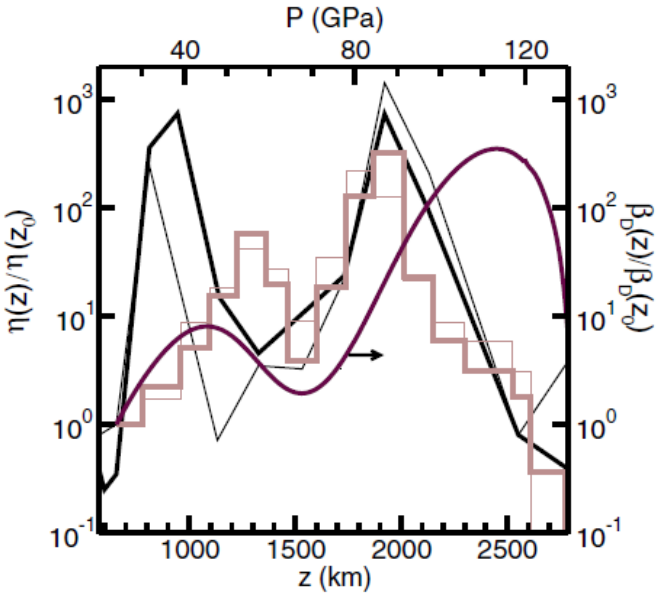

PNAS | May 26, 2009 | vol. 106 | no. 21 | 8447–8452

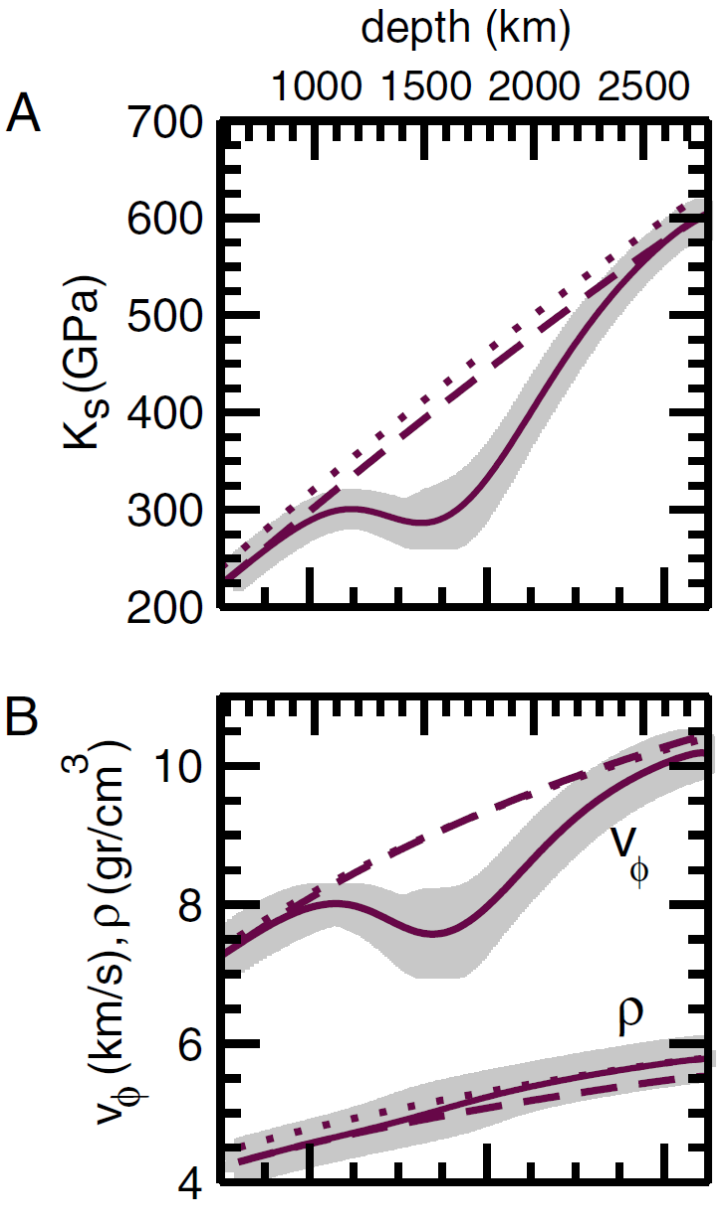

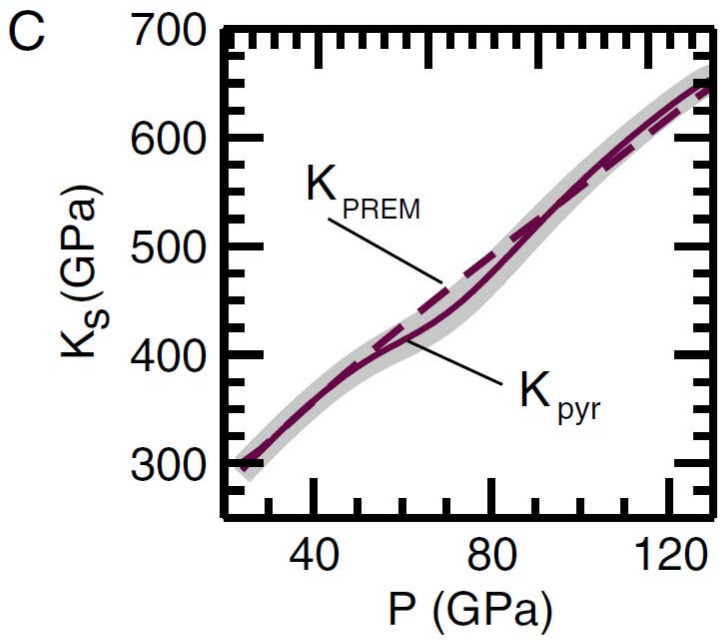

Fig. 3. Properties of $Mg_{1-x}Fe_xO$ ($x = 0.1875$) along a lower mantle geotherm (29). (*A*) Adiabatic bulk modulus, K_S; (*B*) bulk velocity, V_ϕ, and density, ρ; and (*C*) bulk modulus of an aggregate with pyrolite composition, K_{pyr}, compared with PREM's (30) bulk modulus, K_{PREM}. In *A* and *B*, full, dashed, and dotted lines correspond to properties computed in the MS, HS, and LS states, respectively. Shaded regions represent the uncertainties caused mainly by the uncertainty in the computed enthalpies of HS and LS states (see *SI Text*) and spin cross-over pressure at $T = 0$ K.

$$G^*(z) = \delta G_s^*(z) + (1 - \delta) G_D^*(z)$$

where δ is a free parameter. The other quantities are (12):

$$\frac{G_s^*(z)}{G_s^*(z_0)} = \frac{V(z)\mu(z)}{V(z_0)\mu(z_0)} \quad \text{and} \quad \frac{G_D^*(z)}{G_D^*(z_0)} = \frac{V(z)K(z)}{V(z_0)K(z_0)}$$

with $\mu(z)$, $K(z)$, and $V(z)$ being shear and bulk moduli

Physics of the Earth and Planetary Interiors xxx (2011) xxx–xxx

Contents lists available at ScienceDirect

Physics of the Earth and Planetary Interiors

journal homepage: www.elsevier.com/locate/pepi

The impact of variability in the rheological activation parameters on lower-mantle viscosity stratification and its dynamics

Ctirad Matyska [a], David A. Yuen [b], Renata M. Wentzcovitch [c], Hana Čížková [a,*]

$$\frac{\eta}{\eta_{ref}} = \exp\left(12.66\left(\frac{G(z)}{0.15+1.7T}-1\right)\right)$$

$$\begin{aligned}
G(z) &= 1.0 && \text{for} \quad 0.00 \leqslant z \leqslant 0.23,\\
G(z) &= 1.0 + 0.2(z-0.23)/0.19 && \text{for} \quad 0.23 \leqslant z \leqslant 0.42,\\
G(z) &= 1.2 - 0.1(z-0.42)/0.13 && \text{for} \quad 0.42 \leqslant z \leqslant 0.55,\\
G(z) &= 1.1 + 0.7(z-0.55)/0.45 && \text{for} \quad 0.55 \leqslant z \leqslant 1.00
\end{aligned}$$

$$\begin{aligned}
\frac{\alpha}{\alpha_s} &= (1+0.78z)^{-5} && \text{if} \quad 0 \leqslant z \leqslant 0.23,\\
\frac{\alpha}{\alpha_s} &= 0.44(1+0.35(z-0.23))^{-7} && \text{if} \quad 0.23 < z \leqslant 1,
\end{aligned}$$

We have employed a two-dimensional Cartesian model for thermal convection in which the dimensionless stream function and temperature in the extended-Boussinesq approximation (e.g. Steinbach et al., 1989) are employed. The details of this model can be found in (Matyska and Yuen, 2007). We note that the mantle phase changes are set at a given depth within the framework of the effective thermal expansivity formulation (Christensen and Yuen, 1985). The Rayleigh number $Ra \equiv \rho_s^2 c_p \alpha_s \Delta T g d^3 / \eta_{ref} k_s = 10^7$, ($\rho_s$ is the surface density, α_s is the surface thermal expansivity, ΔT is the temperature drop across the mantle, g is the gravity acceleration, d is the depth of the mantle used in the non-dimensionalization, c_p is the specific heat under a constant pressure, η_{ref} is a reference viscosity and k_s is the surface thermal conductivity). The dimensionless internal heating $R \equiv Q d^2 / k_s \Delta T = 3$, where Q denotes volumetric heat sources, which corresponds approximately to one fourth of the whole mantle chondritic heating (e.g. Leitch and Yuen, 1989) because of our Cartesian geometry (O'Farrell and Lowman, 2010). Finally, the surface dissipation number Di used for adiabatic and viscous heatings $Di = \alpha_s g d / c_p = 0.5$ was chosen.

At a dimensionless depth $z = 0.23$, corresponding to a depth of 670 km, endothermic spinel-perovskite phase change was incorporated into all models by means of the buoyancy parameter $P = (\Delta\rho/\alpha_s\rho^2 gd)(dp/dT)$ equal to -0.08(ρ is a reference mantle density, $\Delta\rho$ is the density jump due to the phase change under consideration and dp/dT is the Clapeyron slope). The post-perovskite phase change near the core-mantle boundary at a depth $z = 0.92$, corresponding to a depth of 2680 km, with $P = 0.05$ was considered in the cases, when the ppv phase transition in the D''-layer was taken into account. Computations have been performed in a wide box with an aspect ratio equal to ten. One hundred twenty-nine evenly spaced points were employed in the vertical direction and the same resolution was used in the horizontal direction.

k=1 in the whole mantle, no ppv

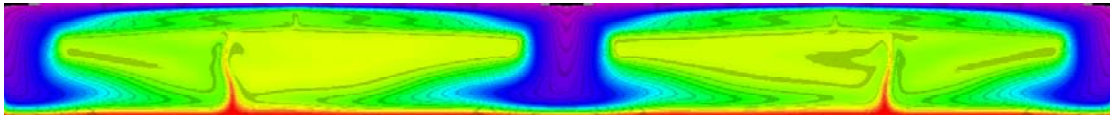

T=0 T=1

ppv layer in D”
k=1 in the whole mantle
no changes of viscosity parameters in ppv

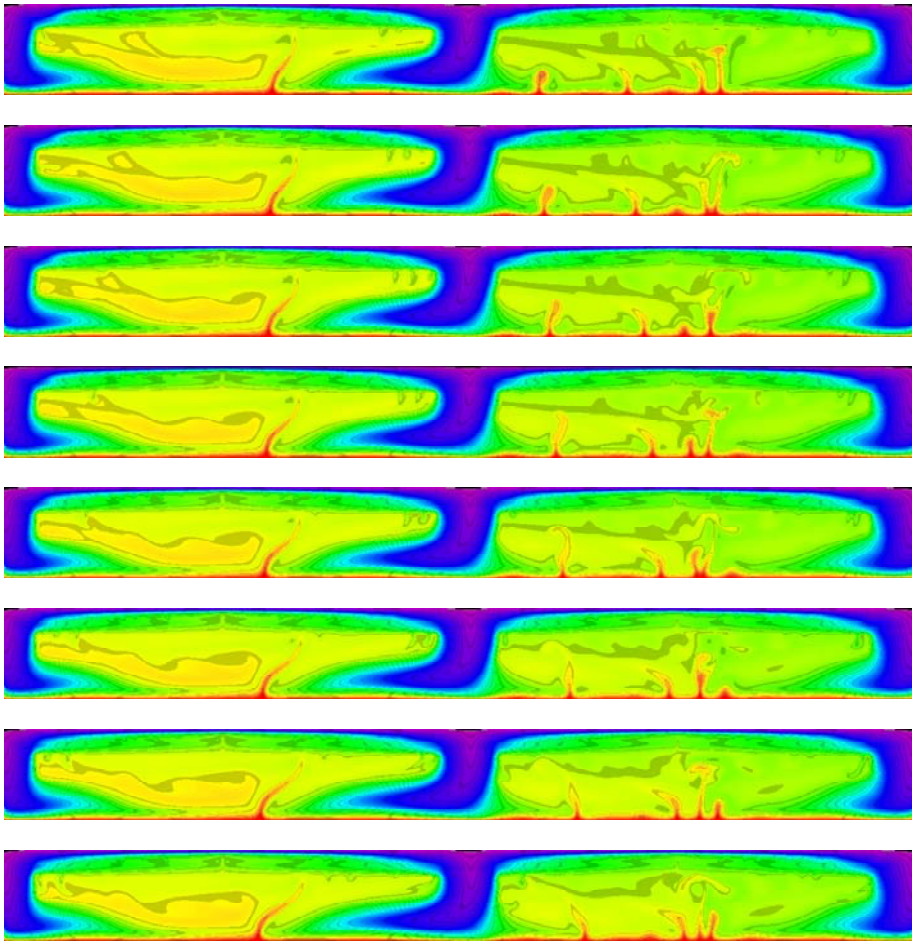

ppv layer in D”
$k=1+T^3$ in ppv, k=1 above D”
no changes of viscosity parameters in ppv

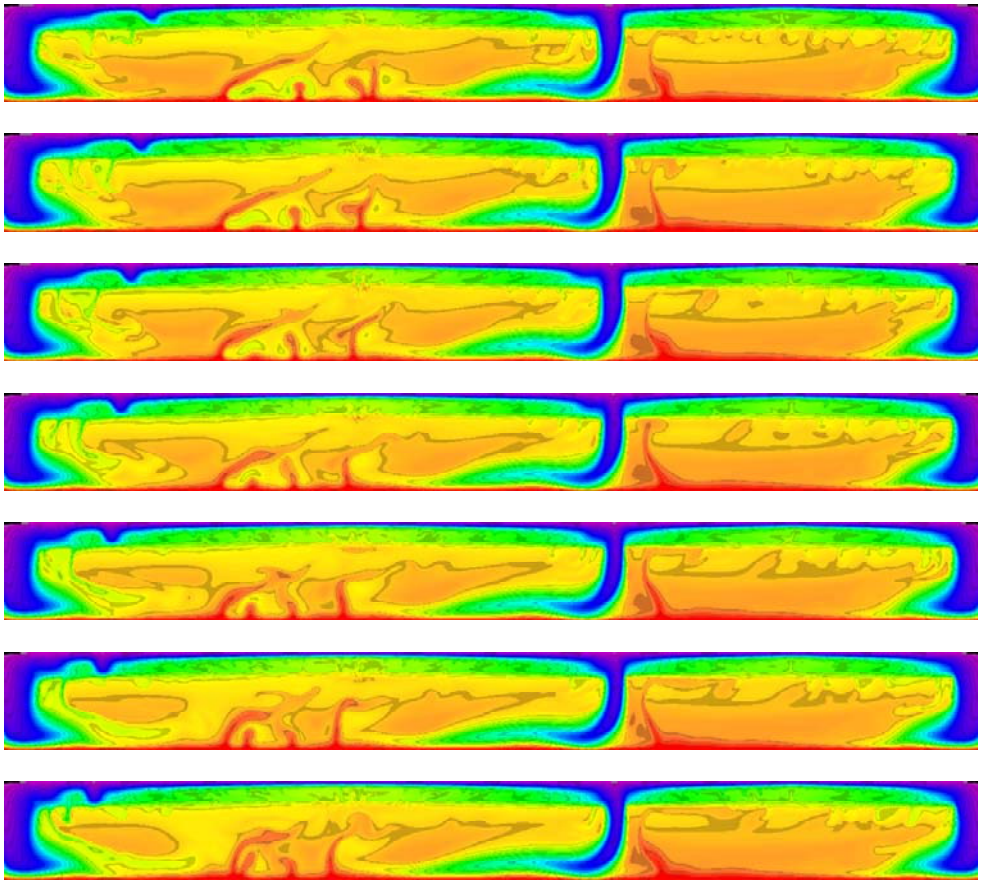

ppv layer in D”
k=1 in the whole mantle
ppv viscosity decreased by one order of magnitude

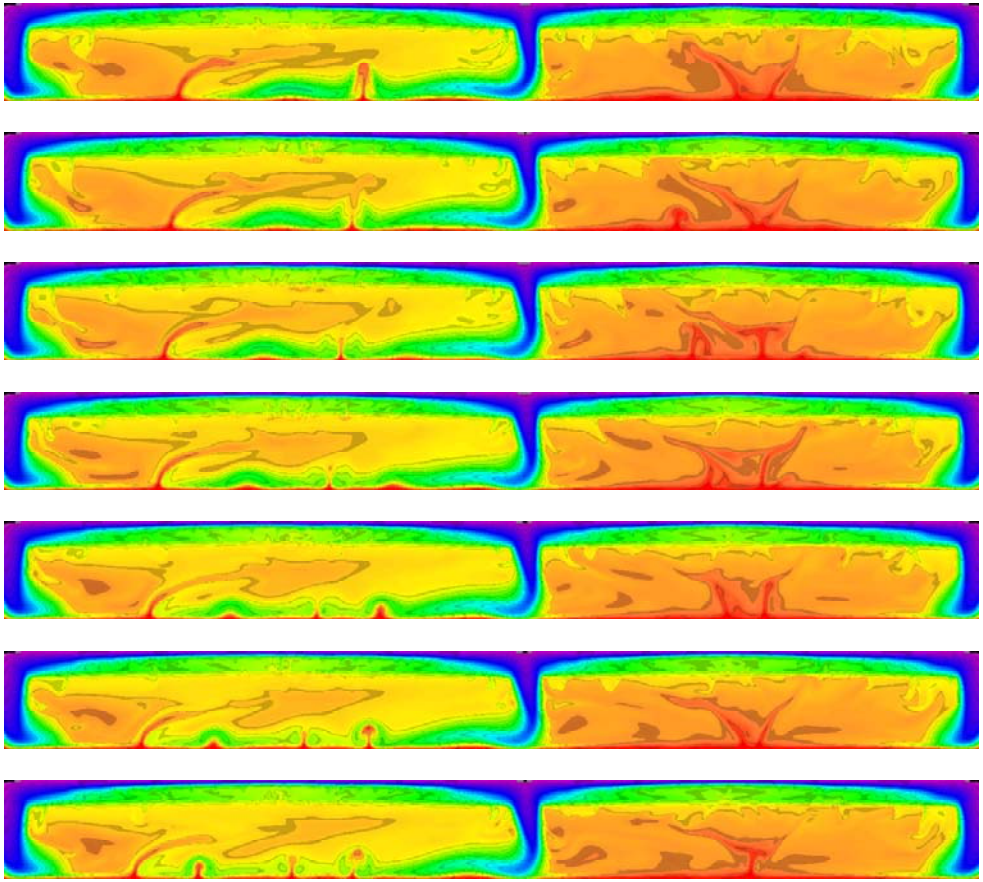

T=0 **T=1**

no ppv, k=1 in the whole mantle

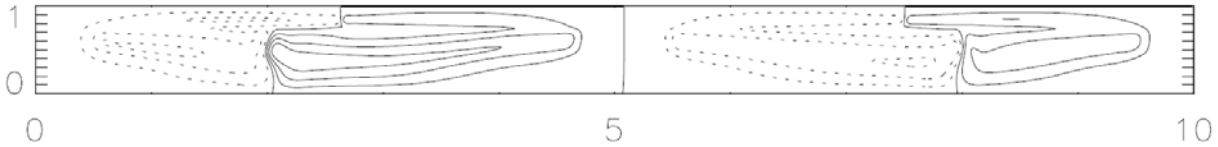

ppv layer, k=1 in the whole mantle, no viscosity changes in ppv

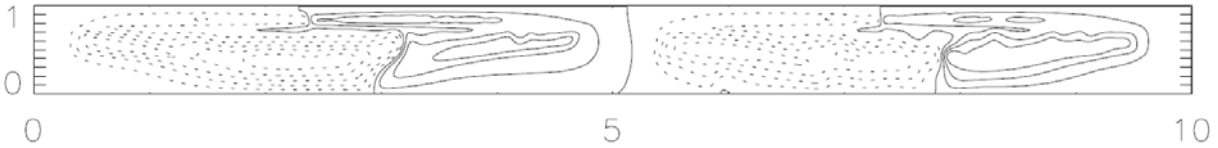

ppv layer, k=1+T^3 in ppv, no viscosity changes in ppv

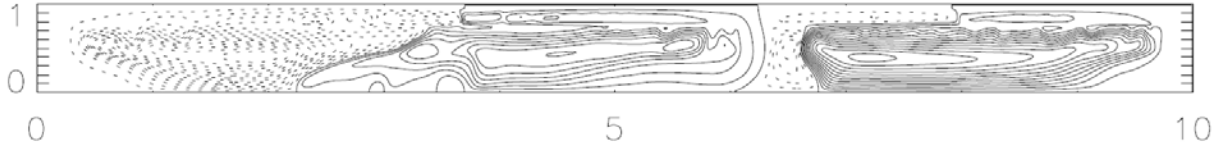

ppv layer, k=1 in the whole mantle, viscosity in ppv decreased by 10

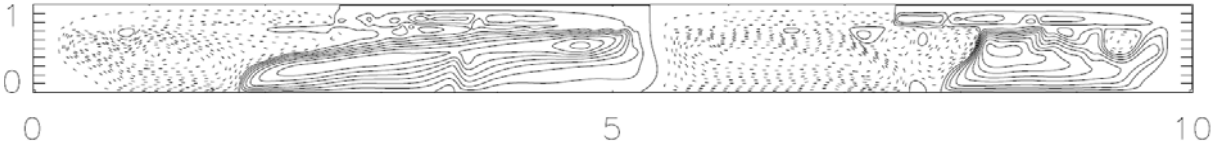

Decadic logarithm of dimensionless viscosity

k=1 in the whole mantle, no ppv

k=1 in the whole mantle, ppv layer, no changes of viscosity parameters in ppv

k=1 above ppv layer, $k=1+T^3$ in ppv, no changes of viscosity parameters in ppv

k=1 in the whole mantle, ppv layer, ppv viscosity decreased by ten

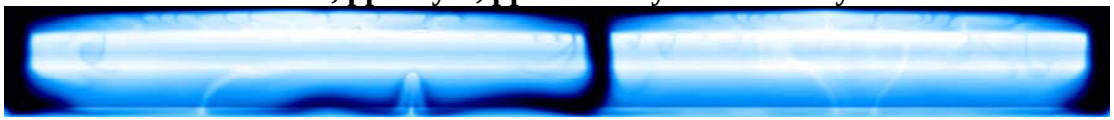

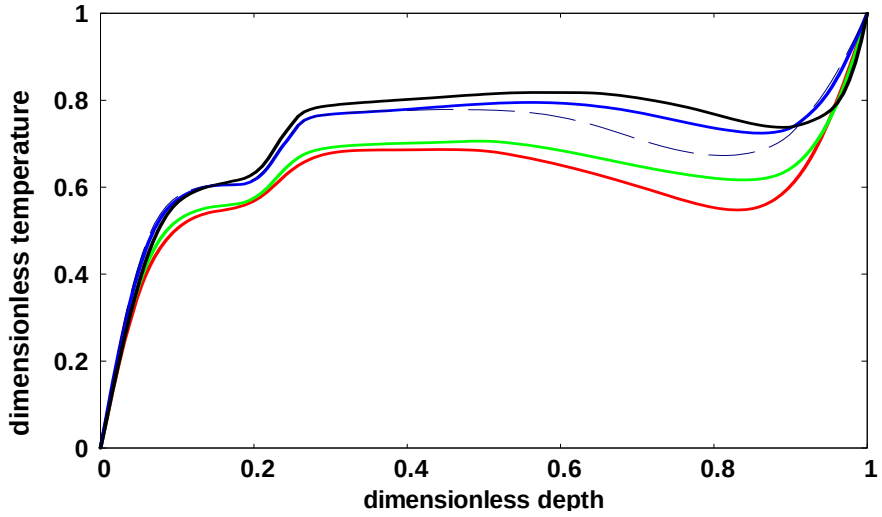

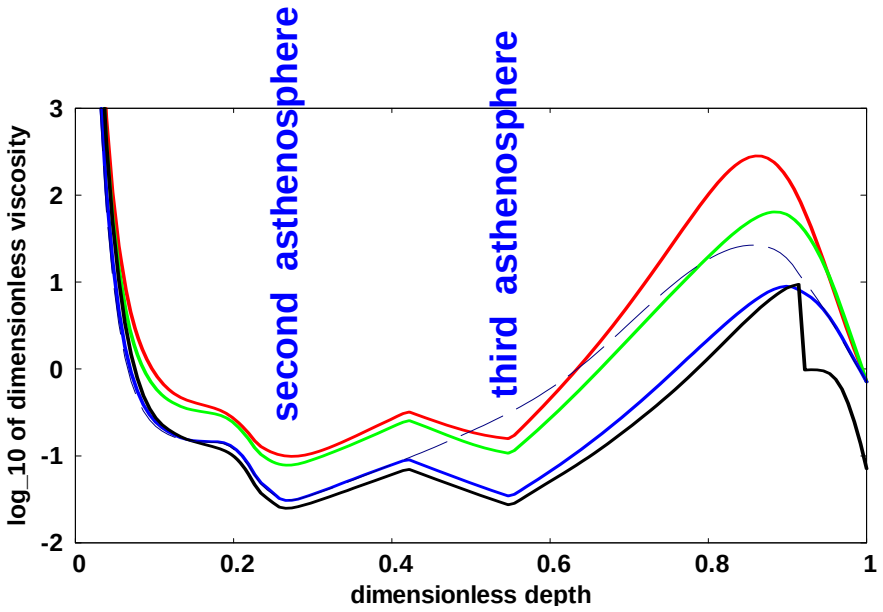

solid lines: original profile of the activation energy

dashed lines: modified profile of the activation energy

red: no ppv, k=1 in the whole mantle

green: ppv layer, k=1 in the whole mantle, no changes of viscosity in ppv

blue: ppv layer, $k=1+T^3$ in ppv and k=1 above D", no changes of viscosity in ppv

black: ppv layer, k=1 in the whole mantle, viscosity in ppv decreased by 10

Enhanced convection and fast plumes in the lower mantle induced by the spin transition in ferropericlase

Dan J. Bower,[1] Michael Gurnis,[1] Jennifer M. Jackson,[1] and Wolfgang Sturhahn[2]

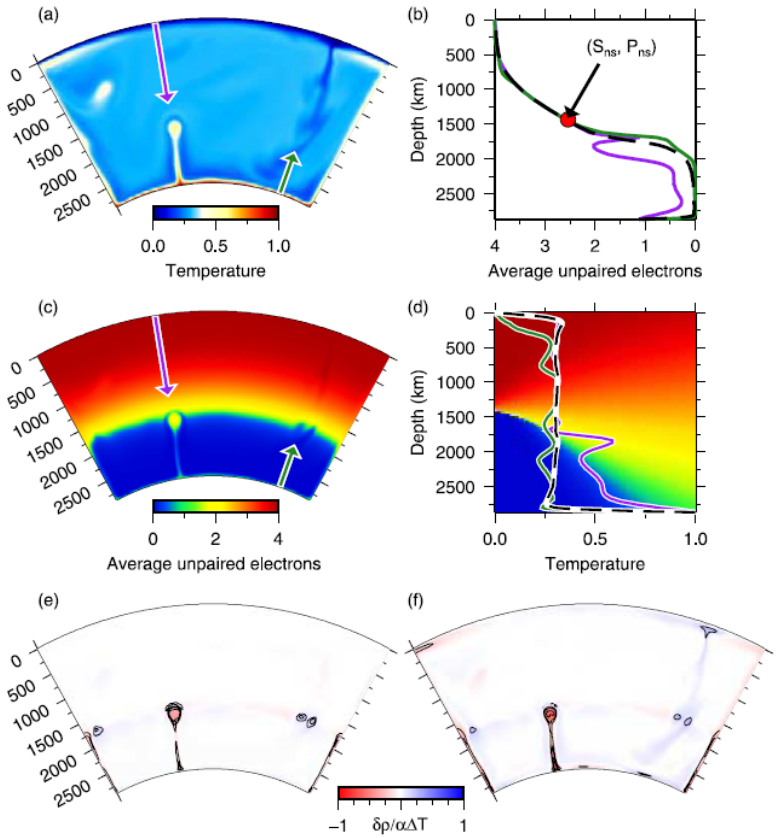

Figure 1. Snapshot from Case 13 at quasi-steady state. (a) Non-dimensional temperature. The purple and green lines delineate the location of representative warm and cold geotherms, respectively. (b) Unpaired electrons (spin-state) for representative warm (purple) and cold (green) geotherms. Red dot is (S_{ns}, P_{ns}) for the spin-state model (see text). Black dashed line is the reference (horizontally-averaged) spin-state. (c) Unpaired electrons with geotherm locations. (d) Geotherms with *Sturhahn et al.* [2005] spin-state model. Black dashed line is the reference geotherm. (e) Spin density anomaly, scaled by $1/\alpha\Delta T$, relative to the horizontally-averaged profile. Contour interval is 0.1. (f) Total density anomaly, scaled by $1/\alpha\Delta T$, relative to the horizontally-averaged profile. Contour interval is 0.2.

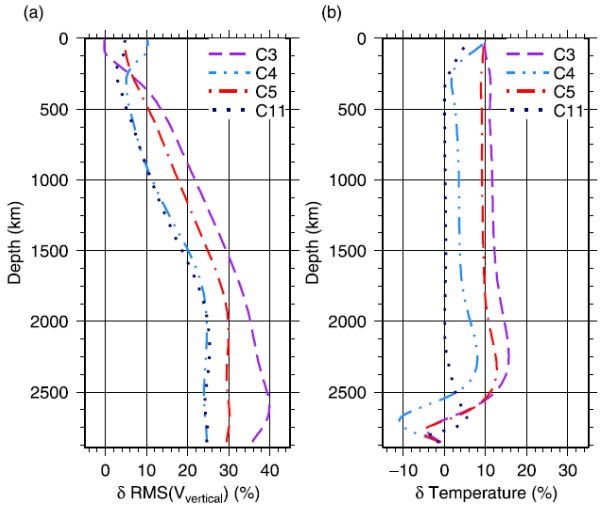

Figure 2. Fractional change (horizontally-averaged) caused by the spin transition (%) for representative cases at quasi-steady state. (a) RMS vertical velocity. (b) Temperature.

Table 1. Input and Output Characteristics of the Models[a]

	Input					Output
Case	*Ra*	*A*	Regime	Nu_n	Nu_s	$\Delta Nu(\%)$
1	5×10^6	0	Steady	11.40	12.47	9.4
2	5×10^6	4	Steady	9.52	10.43	9.5
3	5×10^6	6	Steady	8.79	9.64	9.7
4	1×10^7	0	Steady	11.51	12.65	9.9
5	1×10^7	4	Steady	11.56	12.66	9.5
6	1×10^7	6	Steady	10.54	11.57	9.9
7	5×10^7	0	Steady	19.47	21.15	8.6
8	5×10^7	4	Time-dependent	18.11 ± 0.11	19.10 ± 0.22	5.5
9	5×10^7	6	Time-dependent	13.10 ± 0.61	14.13 ± 0.62	7.9
10	1×10^8	0	Time-dependent	24.39 ± 0.03	26.13 ± 0.43	7.1
11	1×10^8	4	Time-dependent	21.37 ± 0.49	22.67 ± 0.41	6.1
12	1×10^8	6	Time-dependent	16.56 ± 0.64	17.37 ± 1.26	4.9
13	5×10^8	4	Time-dependent	30.55 ± 2.35	31.80 ± 2.33	4.1

JOURNAL OF GEOPHYSICAL RESEARCH, VOL. 116, B08205, doi:10.1029/2010JB007965, 2011

The high-pressure electronic spin transition in iron: Potential impacts upon mantle mixing

M. H. Shahnas,[1] W. R. Peltier,[1] Z. Wu,[2] and R. Wentzcovitch[3]

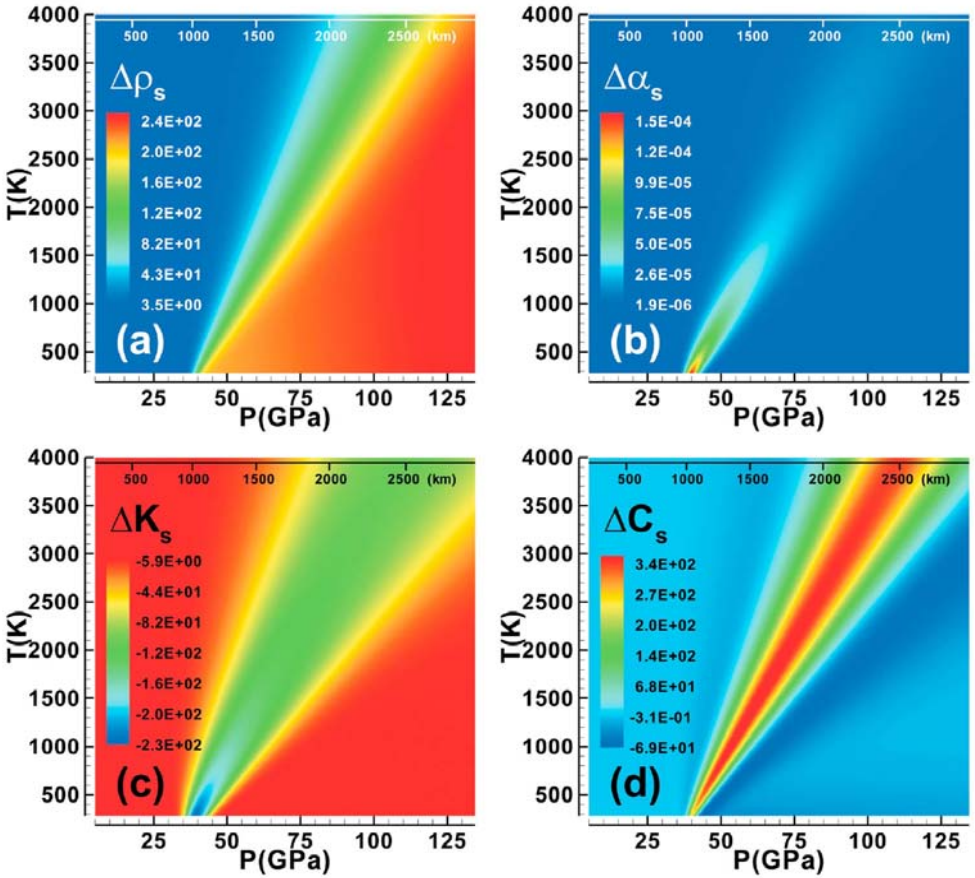

Figure 1. Pressure and temperature dependence of spin-induced anomalies in (a) density in kg/m^3, (b) thermal expansivity in 1/K, (c) bulk modulus in GPa, and (d) heat capacity in J/kg/K in ferropericlase ($Mg_{(1-x)}Fe_xO$) with X = 0.1785. The anomalies are determined by the difference in thermodynamic properties between the mixed spin (MS) state and the HS state [*Wu et al.*, 2009]. The scale represents the depth in the mantle.

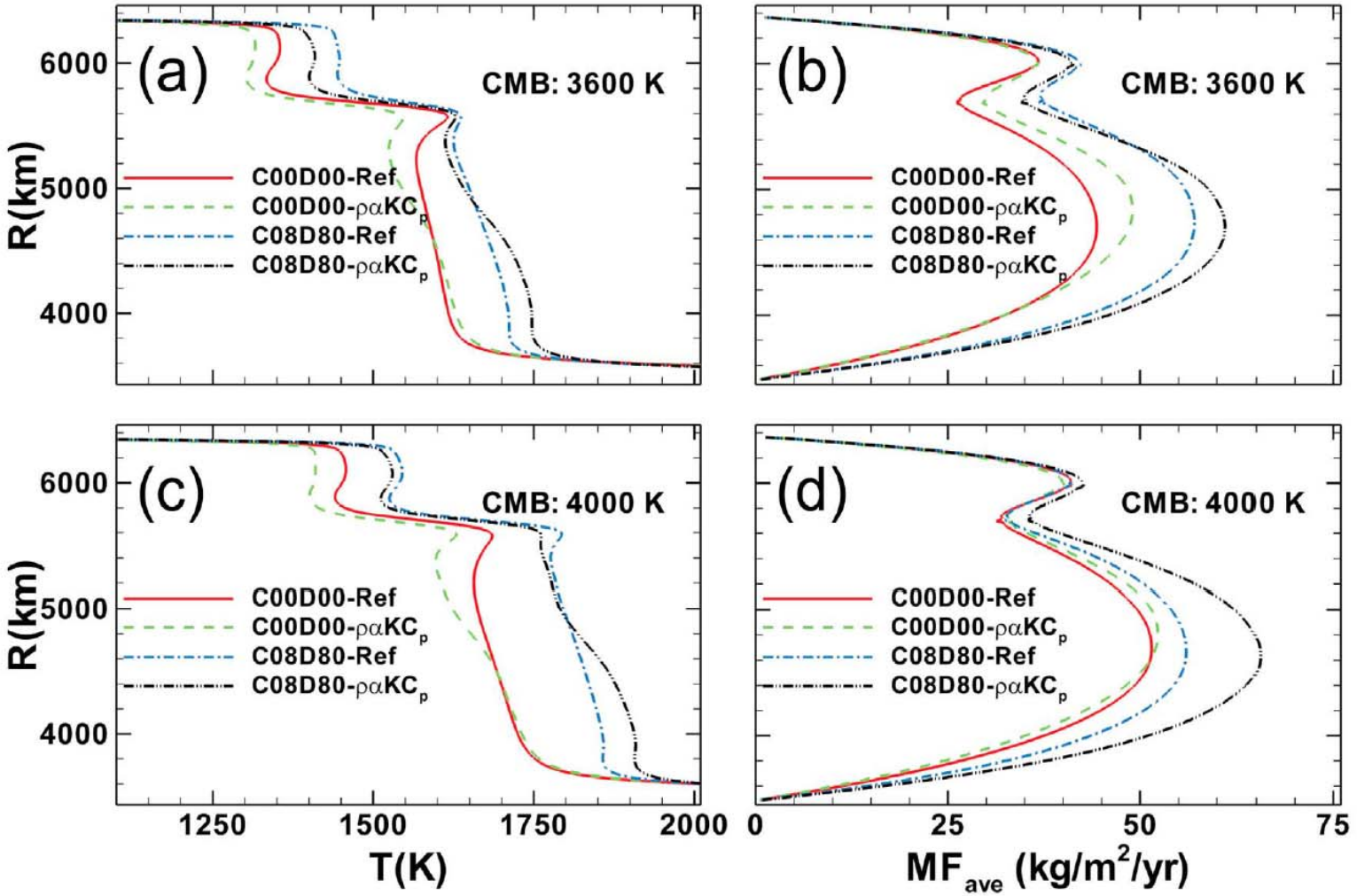

Figure 3. (a) Geotherms for the models with and without Pv–pPv phase transition in the presence of lower mantle spin crossover in ferropericlase (*C00D00 − ραKC$_P$* and *C08D80 − ραKC$_P$*) are compared with the reference model counterparts (*C00D00 − Ref* and *C08D80 − Ref*) with no spin crossover effects (i.e., the models fully in the HS state consistent with PREM mantle density profile) assuming a 3600 K CMB temperature. (b) Time-averaged absolute radial mass flux profiles for the models described in Figure 3a. (c) Similar to Figure 3a but with CMB at 4000 K. (d) Similar to Figure 3b but with CMB at 4000 K.

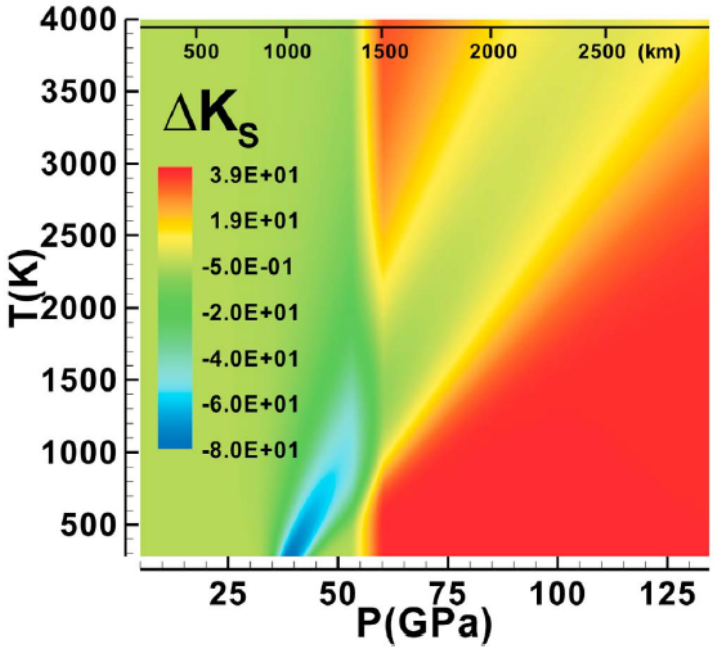

Figure 4. Pressure and temperature dependence of total spin-induced bulk modulus anomaly (in GPa) in ferropericlase and perovskite mixture [*Wu et al.*, 2009; *Catalli et al.*, 2010]. The contributions arising from ferropericlase and perovskite are weighted by a factor of 1/3 and 2/3 respectively in this superposition. The scale represents the depth in the mantle.

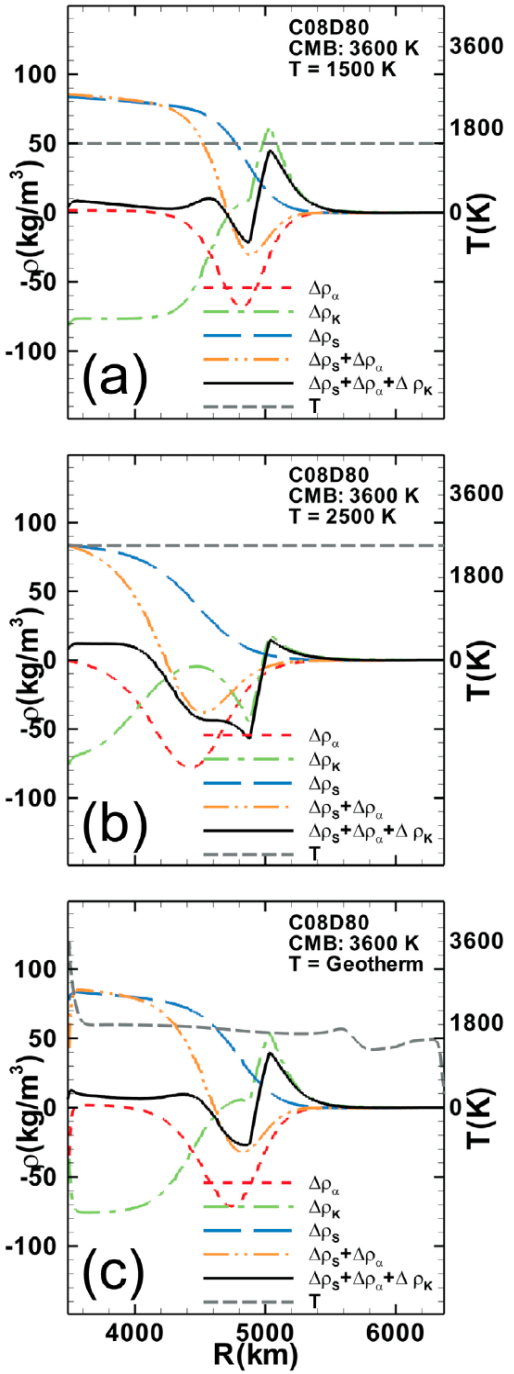

Figure 5. Depth (pressure) dependence of the density anomalies in the models *C08D80* due to the spin crossover in the lower mantle as discussed in the section 4.2 for (a) a low temperature of 1500 K, (b) a high temperature of 2500 K, and (c) a sample mantle geotherm. The spin-induced anomaly in bulk modulus $\Delta\rho_K$ is a superposition of the bulk modulus anomalies in ferropericlase (Figure 1c) and perovskite weighted by 1/3 and 2/3 respectively as displayed in Figure 4. The model assumes no spin-induced anomalies in density and thermal expansivity components ($\Delta\rho_s$, $\Delta\rho_\alpha$) in the perovskite component of mantle mineralogy and the anomalies arising in ferropericlase component are based on Figures 1a and 1b (weighted by 1/3).

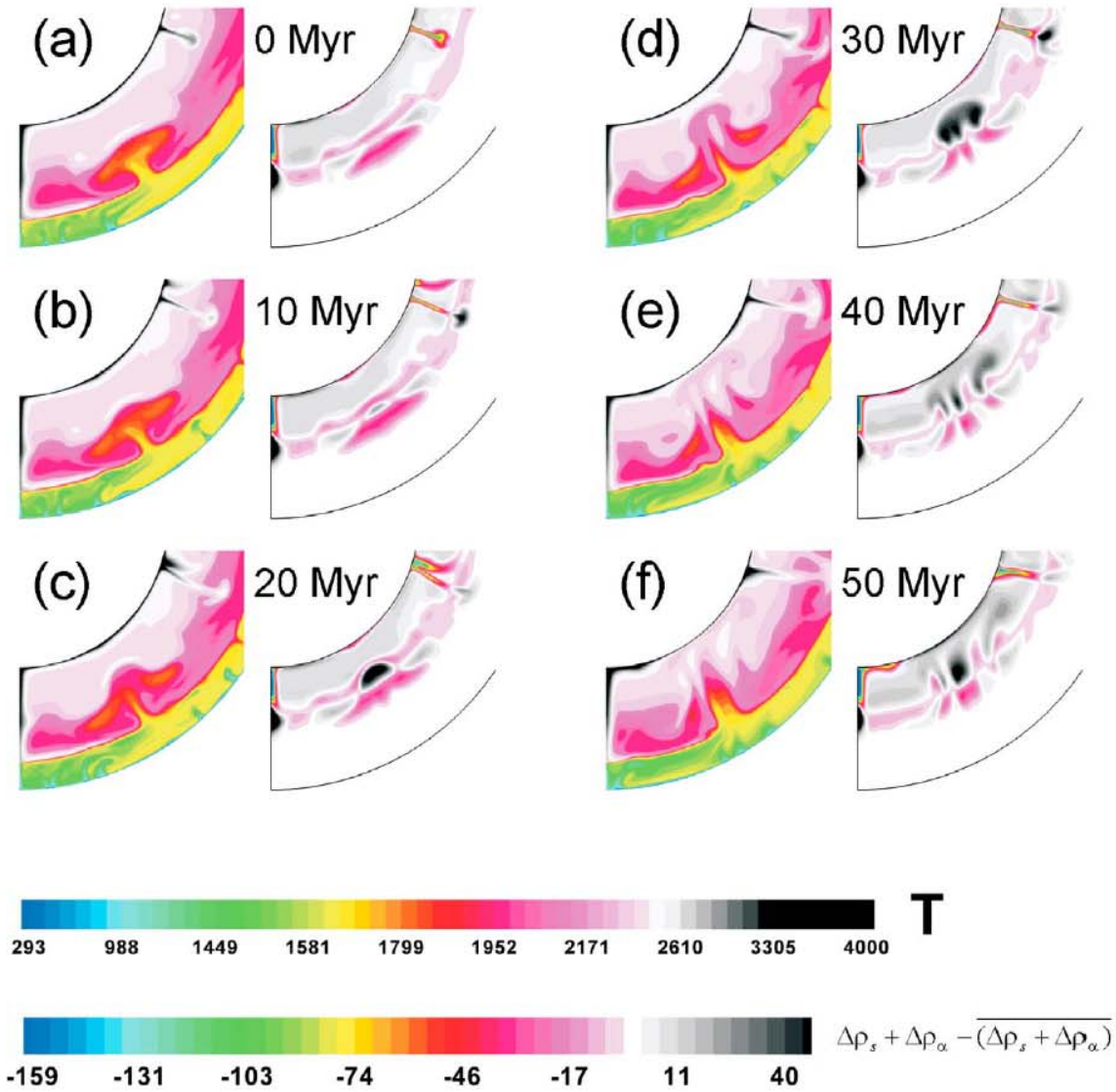

Figure 9. Snapshots of the spin-induced midmantle avalanche (SIMMA) event in the model *C08D80* − $\rho\alpha$ (CMB at 4000 K) described in section 4.4 in 10 Myr intervals. The first and second images at each snapshot show the temperature and spin-induced anomaly of $\Delta\rho_s + \Delta\rho_\alpha$ form which the laterally averaged anomalies have been subtracted at each grid point (i.e., $\Delta\rho_s + \Delta\rho_\alpha - \overline{(\Delta\rho_s + \Delta\rho_\alpha)}$) respectively.